Icarus 410 (2024) 115908

Contents lists available at ScienceDirect

Icarus

journal homepage: www.elsevier.com/locate/icarus

Research Paper

"Cold capture" of micrometeorites in Archean and Quaternary atmospheres: Effects of dilute exospheres

R. Skartlien [a,d,*], J.B. Kihle [a], J. Larsen [b], J.K. Eager-Nash [c], T.L. Palmer [d], T.J. Boxer [f], S.J. Daines [e], N.J. Mayne [c]

[a] Institute for Energy Technology, Instituttveien 8, Kjeller, 2007, Norway
[b] University of Oslo, Project Stardust, Department of Geosciences, Sem Sælands vei 1, Oslo, 0371, Norway
[c] The University of Exeter, Department of Physics and Astronomy, Exeter, EX4 4SB, Devon, UK
[d] Venabo Analytics, Kirkeveien 96, Fetsund, 1900, Norway
[e] The University of Exeter, Exeter, EX4 4PY, Devon, UK
[f] The University of Exeter, Department of Natural Sciences, Exeter, EX4 4SB, Devon, UK

ARTICLE INFO

Keywords:
Unmelted micrometeorites
Amino acids
Archean atmosphere
Remnant atmosphere envelopes

ABSTRACT

Micrometeorites (MM) that undergo low heating could have provided a source of organic material to the Earth during the Archean (4-2.5 Ga ago) before life emerged, given that the density of interplanetary dust and larger grains were much higher than today. Amino acids are destroyed on atmospheric entry if the temperature rises above the pyrolysis temperature of few hundred degrees Celsius, depending on type of amino acid. A numerical study was carried out to obtain temperature statistics along relatively rare grazing angle trajectories in the Quaternary (modern) and Archean atmospheres to determine the probability of "cold capture" below pyrolysis temperatures. Effects of the thermospheric temperature and density was considered for the Quaternary atmosphere, and an extended hydrogen/helium envelope remnant from the protosolar nebula was considered for the Archean atmosphere.

An important result for the Archean is an elevated "cold capture" probability (twice the capture probability of the modern atmosphere, up to 7%–8%) for low heating below 500 °C of small asteroidal grains around 20 μm in diameter, and geocentric velocities in the range 3–5 km/s, provided that there was a remnant envelope. Cometary 20 μm grains of higher geocentric velocities did not have such an elevated capture probability. If the Archean atmosphere did not have an envelope, it was found that these capture probabilities were lower than for the modern atmosphere for both cometary and asteroidal grains, due to smaller density scale height of the lower Archean atmosphere leading to faster heating rate. Radiative degradation of amino acids in these relatively small grains should be considered more closely since the X-ray and XUV-flux from the Sun was larger by a factor of about 5–10 in the Archean.

Very low maximum temperatures were found for 20 μm asteroidal and cometary grains in the Quternary atmosphere, with temperatures in the range 150–200 °C, but with a very small capture probability in this range of typically less than 0.3%. All 300 μm asteroidal grains were heated to temperatures above 500 °C for all atmosphere models. The probability of heating to temperatures < 500 °C of 100 μm asteroidal grains, was estimated to 0.3% or less for all models. Most 100 μm cometary grains were heated to temperatures > 500 °C for all models.

1. Introduction

It is probable that life on Earth emerged in water with an abundant supply of amino acids as the essential building blocks for proteins and enzymes. Did the amino acids form on the Earth or did they come from space carried by meteorites or dust? Amino acids and other biochemical monomers can be produced from reduced gas mixtures such as H_2O, CH_4, H_2 and NH_3 or N_2, as shown by the famous Miller–Urey experiment. However, a weakly reducing or neutral atmosphere is more in agreement with most current models for the early Earth, with a dominance of CO_2 and N_2, and this makes it difficult to explain synthesis of amino acids on Earth without any other additives. Cleaves et al. (2008) argued that synthesis from neutral atmospheres may be more important than previously thought, and significant amounts

* Corresponding author at: Institute for Energy Technology, Instituttveien 8, Kjeller, 2007, Norway.
E-mail address: roar.skartlien@ife.no (R. Skartlien).

https://doi.org/10.1016/j.icarus.2023.115908
Received 23 August 2023; Received in revised form 2 November 2023; Accepted 28 November 2023
Available online 29 November 2023

of amino acids could still be produced in the presence of oxidation inhibitors, such as ferrous iron.

Exogenous or extraterrestrial delivery from space via interplanetary dust, grains from comets and asteroids, and larger meteorites may alleviate the problem of a neutral or weakly reducing atmosphere, and is an alternative route for supplying organic material to the surface of the Earth (Glavin and Bada, 2001). Carbonaceous chondrite meteorites have high concentrations of carbon and contain organic compounds including amino acids, and an increasing number of amino acids have been identified in the Murchison meteorite, with a total of 86 by 2017 (Koga and Naraoka, 2017). Canepa (2013) showed that a constant supply of extraterrestrial amino acids to the oceans of the early Earth could allow for the spontaneous formation of catalytic polypeptides without prior complex RNA-based chemistry (assuming the present day volume of the oceans). Supply of amino acids was found to be one of the key parameters regulating the maximum length of polypeptide chains that could spontaneously form in the primordial ocean (Canepa, 2016).

It has been estimated that about 30 000 tons/year of interplanetary dust particles (IDP) from microns and up to millimeter size is accumulated by the Earth each year, and that 300 tons/year is subject to heating of less than 600 Celsius (Flynn 2004). The results of Carrillo-Sánchez et al. (2016) indicate that the Jupiter family of comets (JFC) contributes with a large fraction of the input mass with (43 ± 14 tons/day) or 15 700 tons/year to the top of the atmosphere. Updated values from Carrillo-Sánchez et al. (2020) indicate JFC mass flux contributions of 70% for Earth, 68% for Venus, and 52% for Mars, providing a total of 28 ± 16 tons/day 31 ± 18 tons/day, and 2 ± tons/day, respectively. The mass contribution of asteroidal dust particles were found to be 9% for Earth, 6% for Venus, and 14% for Mars. According to Anders (1989) and Glavin and Bada (2001), IDP's supply the Earth with $3-40\times10^5$ kg/year (300–4000 tons/year) of carbonacious material (assuming 10 percent organic carbon by mass in IDP's). This flux may have been 5×10^7 kg/year (50 000 tons/year, or roughly between 10 and 100 times larger) during the late heavy bombardment 4.1-3.8 Ga ago (Chyba and Sagan, 1992). Hence, IDP's could potentially have been a source of pre-biotic organics in addition to larger meteorites.

A major problem with MMs larger than about 100 μm is heating to very high temperatures due to friction. Entry velocities are typically in the range from the escape velocity of 11.2 km/s to about 70 km/s, depending on the orbital parameters. Several MM models have predicted typical heating to well above 1500 °C, and Farley et al. (1997) estimated that less than 1% of the total mass of IPD's are heated to less than 600 °C, and that the total mass is essentially zero for heating below 400 °C. The peak mass flux entering below 650 °C was found at to occur at 20 μm diameter. Amino acids in MM are likely to be completely destroyed above 500-600 °C, and Weiss et al. (2018) found that the eight amino acids G, C, D, N, E, Q, R and H that are essential to life are decomposed at quite low temperatures between 185 °C and 280 °C. These experiments were performed with pure amino acids. The degradation temperature of amino acids in meteoritic material may be higher, depending on the interaction forces between the material and the amino acids, and Anders (1989) assumed an average pyrolysis temperature for organic compounds in meteorites of 900 K, or 627 °C. Glavin et al. (2004) performed amino acid analyses of antarctic MM (AMM) and found that less than 5% of all AMMs in the 50–400 μm size range contain detectable levels of AIB (α-aminoisobutyric acid). The authors argued that if AIB is abundant in micrometeorites prior to their fall to Earth, then the lack of AIB in AMMs suggests temperatures > 550 °C in this size range. Glavin and Bada (2001) found that all amino acids in the Murchison meteorite were destroyed at 550 °C. Simulation of micrometeoroid trajectories by Canepa (2020) in the size range 10–70 μm indicated significant retention of glycine for geocentric velocities below about 3 km/s, assuming an incidence angle of 45 degrees, and the corresponding maximum temperatures were about 500 K or 227 °C. Based on the information above we assume that temperatures above 300 °C corresponds to the onset of degradation of some amino acids, and temperatures above 500 °C corresponds to degradation of most amino acids delivered by MM's.

The outlook for surviving amino acids delivered from space in MM then appears to be relatively grim due to the low fraction of trajectories that undergo low heating. However, the probability increases for smaller MMs with diameter less than 100 μm, and the exact numbers depend on the atmospheric density profile. This small fraction of trajectories with grazing angle incidence and low heating may also explain why less than 5% of all AMMs in the study of Glavin et al. (2004) contained amino acids. In the context of the origin of life during the Archean, the atmospheric density profile was different than in the current atmosphere, with the dominance of CO_2 and N_2 and with the possibility of a remnant and very dilute hydrogen/helium envelope extending to several Earth radii (Lammer et al., 2014). One would expect higher capture probability of MM that undergo low heating with such an envelope. The main focus of the current work was to determine the temperature statistics of unmelted MM for different atmospheric density profiles, with special focus on the Archean.

An alternative route of delivery is sublimation of amino acids from the MM surface before significant heating of the MM occurs. Amino acids have relatively high vapor pressure and can sublime under low pressure conditions above about 150 °C. Glavin and Bada (2001) studied sublimation of glycine (G) from the Murchison meteorite material and argued that sublimation is a way for amino acids to survive (or escape) atmospheric entry heating. The sublimated amino acids might combine with ice crystals, despite that the mesosphere and stratosphere are presently extremely dry, and then spend most of their time in sulfate aerosol that finally rain. Current stratospheric aerosol show that about half of the particles contain 0.5 to 1.0 weight percent meteoritic iron by mass (Cziczo et al. 2001). This transport mechanism could also work in the Archean but the aerosol and moisture contents in the Archean atmosphere are uncertain.

A third route of delivery is larger meteorites that may only experience significant heating in the surface layers on the journey through the atmosphere depending on size, heat conduction, and the duration of the heating pulse. The interior chonditric material may keep a sufficiently low temperature, but he main bottle neck with the larger meteorites is impact heating. Bertrand et al. (2009) studied the effect of ground impact heating on amino acids.

1.1. Examples of micrometeorites

Micrometeorites can also be collected in urban areas, as demonstrated by J. Larsen and collaborators (Larsen, 2016; Genge et al., 2017). These display a large variety of heating histories, and Fig. 1 shows three examples of MM with diameters close to 300 μm. They were magnetically extracted from urban roof tops by J. Larsen, and the samples were filtered according to size, and then manually sorted under a microscope (Larsen, 2016). Top left: (a) NMM 2752 heated to above 2000 °C. It consists of melted glass with a thin crystallized zone towards a sulfide edge which borders to a nickel-iron alloy (on the top). (b) NNM 2081 (top right) of barred olivine with yellow-white platina nuggets, heated to 1800 °C. Specimen (c), NMM 2123 (bottom left), is a good candidate for a MM that has experimenced a grazing angle, low heating trajectory. It is characterized by partial melting with an irregular, but aerodynamic shape, and a crystallized glass-protuberance. The glass protuberance at the top has probably been formed by air friction dragging the melted surface layers to the back, before crystallizing. Genge et al. (1996) found textural indications for grazing angle incidence with at least two aero-breaking events for a similar glassy spherule found in Antarctica. This MM had a glass core with four peripheral glass lobes. The peak temperature in the first pass was estimated to 1400 °C or more, for melting and formation of an internal glass spherule. The peak temperature in the second pass was estimated to below 1100 °C based on surface textures. This particular

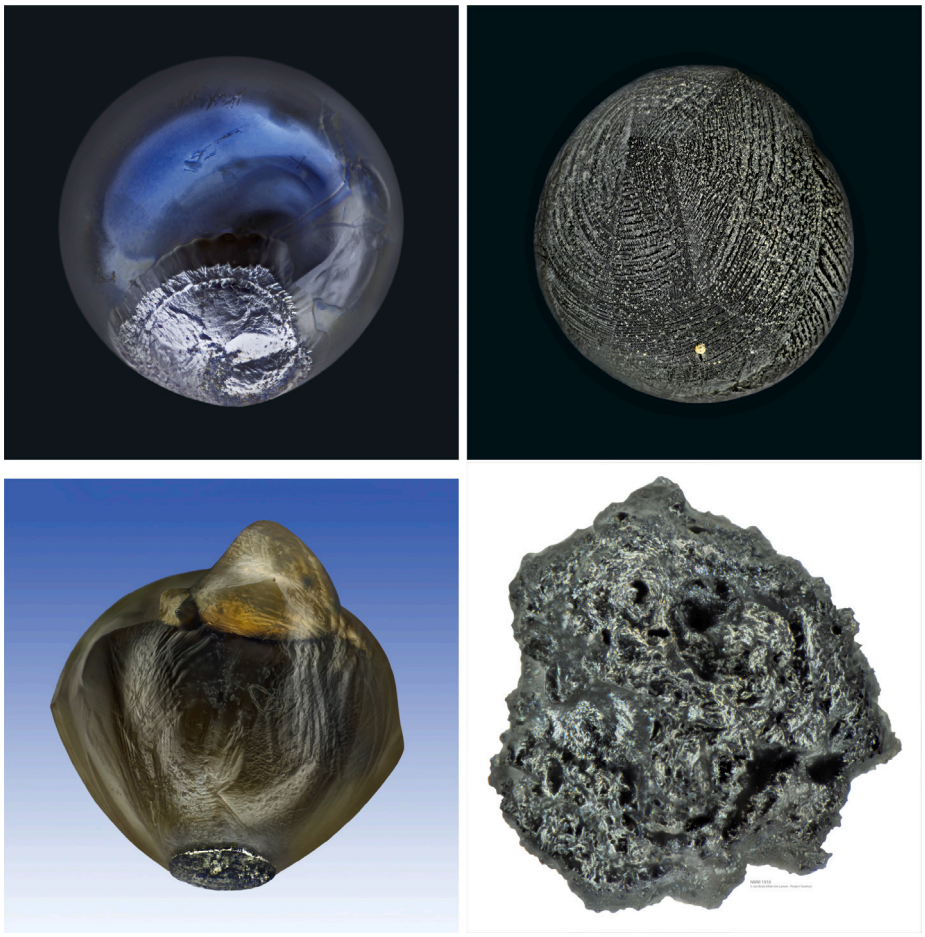

Fig. 1. Micrometeorites collected from urban roof tops by J. Larsen. Top left: (a) NMM 2752 (melted glass) heated to above 2000 °C. Top right: (b) NNM 2081 (barred olivine) heated to about 1800 °C, with multiple yellow-white platina droplets. Bottom left: (c) Grazing angle candidate NMM 2123, with partially melted glass forming an aspherical irregular shape, with estimated heating up to 1400 °C. The decelerating force has been acting upwards (moving downwards), with heavy elements sinking to the front, forming a metal bead. Bottom right: (d) NMM 1918 is a grazing angle candidate of the *unmelted* type, and it has been heated to less than 1350 °C. It must be noted that only unmelted MM can deliver organics to Earth. (For interpretation of the references to color in this figure legend, the reader is referred to the web version of this article.)
Source: Images by J. B. Kihle and J. Larsen.

MM had a diameter of 60 μm, and possibly a high entry velocity in excess of 20 km/s, suggesting cometary origin.

Strictly unmelted MM must have been subject to temperatures below 1000–1500 °C depending on composition (Genge, 2017) (the melting temperature is about 1200 °C for chondrites), and the probability of finding unmelted MM is relatively low in general, since less than a percent of the MM being captured by the Earth have low temperature grazing angle trajectories (Genge et al., 1996). Many unmelted MM with highly irregular shape and a porous character, have been found in Antarctica (Engrand and Maurette, 1998; Taylor et al., 2000; Duprat et al., 2007; Genge et al., 2008; Folco and Cordier, 2015), and some of these MM have also proven to contain organic compounds.

Variety (d), NMM 1918 (bottom right Fig. 1), is a rare unmelted micrometeorite, high in carbon/organics (preliminary analysis), heated to less than 1350 °C. Micrometeorites that can preserve amino acids are subject to even lower temperatures, below about 500 °C, and the probability of finding these "colder" types is relatively low as we shall see. This raises the question if the organic contents in these MM had any significance for the development of life on Earth, compared to organics from larger meteorites, or from endogenous sources (e.g., underwater thermal vents).

1.2. Atmospheric entry modeling

Many authors have carried out trajectory calculations under a few justified assumptions. The mean free path of gases is larger than the MM size in the upper atmosphere (high Knutsen number, Kn) and the drag force is now purely kinetic due to the change of momentum of the molecules when they hit the MM surface. A bow-shock will not be formed, since the impinging gas molecules bounce back with no or little interaction with incoming gas. Most authors have considered nearly or complete inelastic collisions in their simulation models (e.g., Flynn, 1989a; Love and Brownlee, 1991), and the kinetic energy of the incoming gas molecules is converted to thermal energy in the MM material. Some material sublimates or ablates and provides a heat sink together with radiation cooling. Solar heating maintains a temperature in vacuum of a few degrees Celsius at 1AU, assuming that the MM is effectively a black-body. The temperature evolution can be calculated, given the heat capacity of the MM, together with parameters associated with the saturation vapor pressure during sublimation or ablation. Ablation did not occur for the low temperature scenarios we studied here.

Most entry models assume a spherical representation of micrometeoroids, and isothermal interiors (Folco and Cordier, 2015). This is however a coarse simplification since MM's show a range of textures, shapes and mineral compositions, and a range of heat conduction and heat capacities. Cometary grains can also be porous and heterogeneous with implications for heat capacity and heat conductivity. The heat capacity determines the timescale of heating, and the temperature lags the heating rate more for larger heat capacity, and the effect will be more significant for shorter heating pulses (steeper descent). Approximate equilibrium is more likely for grazing angles with longer heating

duration. Flynn (1989a), Love and Brownlee (1991) considered high Kn-number friction and assumed instantaneous thermal equilibrium, and inelastic collisions with gas molecules. Genge (2017) followed a similar approach but solved for the temperature history rather than assuming equilibrium. All authors considered isothermal MM with a drag force based on circular cross sections.

The Lorentz force for 0.1 μm grains is comparable to radiation pressure and gravity, while it is a minor perturbation for 1 μm grains according to Horanyi et al. (1988). One can then safely ignore the Lorentz force in the magnetosphere for sizes larger than 1 μm, and the radiation pressure force is orders of magnitude smaller than gravity. Hence, it is sufficient to consider only friction and gravity in the equation of motion for grains in the size range we studied (from 20 μm and up).

Most trajectory modeling efforts in the past considered the current atmosphere, with a few exceptions. Lehmer et al. (2020) studied chemical synthesis on the MM surface during descent in CO_2-rich Archean atmospheres. Lighter gases in the current atmosphere do have an impact on satellite drag, including very dilute and extended hydrogen and helium envelopes, despite the fact that these gases are slowly depleted over time by diffusion into space. Hence, one would expect a larger effect of these gases on drag in the Archean atmosphere if it had a significant hydrogen and helium exosphere.

2. The trajectory model

We also assume non-equilibrium temperature evolution, isothermal conditions throughout the MM, spherical shape, and with the possibility of sublimation. We focus on grazing angle trajectories only, and incorporate any multi-aerobraking history until descent. A precise tuning of the initial conditions is required to realize a sufficient number of trajectories in the narrow entry corridor that corresponds to grazing trajectories and descent. Previous work often limited the number of passes through the atmosphere (terminating the calculations after a fixed number of passes, before descent could occur) mainly to reduce the computational load. The current work can be regarded as a generalization where all MM are tracked until descent to the Earths surface occurs. The computations are made efficient by incorporating adaptive timestepping with large time steps in vacuo and small time steps in the atmosphere. This enables continuous trajectory simulations to avoid book-keeping with respect to exit and entry conditions into the atmosphere, and it allows for the inclusion of very dilute extended atmospheric envelopes. The time-step in vacuum was controlled by the local acceleration, with gradually diminishing time steps closer to the Earth. A small fixed time-step was used in the atmosphere, and a density-dependent weighting was performed between these two limits.

2.1. The model equations

The standard fourth order Runge–Kutta method was used for integrating the equation of motion and the thermal energy equation, including ablation and radiation. The equation of motion involves solving for position given the velocity, and solving for the velocity given the acceleration. These two equations must be staggered in the RK4 schema to evaluate the four intermediate derivatives and to obtain sufficient accuracy. This approach in combination with adaptive time-stepping was tested on Keplerian orbits in the two-body problem to ensure energy conservation to very high accuracy. Friction was then added, and the solver was then tested for correct terminal velocity during the vertical descent phase. The acceleration in the low Kn-regime is given by (Love and Brownlee, 1991; Genge, 2017)

$$\dot{\mathbf{v}} = -\frac{4}{3}\frac{\rho_a(t)}{\rho_p}\frac{1}{r_p(t)}|\mathbf{v}|\mathbf{v} + \frac{\mu}{|\mathbf{R}|^3}\mathbf{R}, \tag{1}$$

where $\mathbf{R}$ is the radius vector from Earth's center, $\mu = GM$, where M is the mass of the Earth, ρ_a is the atmospheric density at the particle position and r_p is the MM radius. The latter two are generally time dependent as the particle experiences higher gas density as it descends and the radius decreases if the material sublimates. At sufficient atmospheric density, the mean free path of the gas molecules is reduced with increasing collision frequency, and the drag term must be derived from fluid dynamics, not kinetics. This has no consequence for the study if the heating phase is completed before these lower altitudes are reached where the Knutsen number is of order unity.

Table 1
Grain parameters.

	Asteroidal grains	Cometary grains
Geocentric velocity v_∞	3 km/s 5 km/s 7 km/s	12 km/s 15 km/s 18 km/s
Density ρ_p	3.4 g/cm^3	1 g/cm^3
Diameter $2r_p$	300 μm, 100 μm, 20 μm	100 μm, 20 μm

For the low temperature scenarios we studied, none of the MM's sublimated, and the radius stayed constant. The orbit and temperature history is then the same for all particles that satisfy the same size-density product. The energy equation depends on the mass loss rate, MM volume, and radiative heating and cooling. These two equations were also staggered according to the RK4 schema. The internal energy equation in terms of temperature T can be written (e.g., Genge, 2017)

$$r_p(t)\rho_p C\frac{\partial T}{\partial t} = \frac{3}{8}\rho_a(t)|\mathbf{v}|^3 + 3L_v\frac{\partial r_p}{\partial t} - 3\sigma\epsilon T^4 + \frac{3}{4}P_{solar}, \tag{2}$$

where C is the heat capacity, L_v is the latent heat of sublimation, σ is the Stefan–Boltzmann constant representing isotropic radiation cooling, ϵ is the radiative emissivity. P_{solar} is the solar radiative flux density at 1AU, with a current average value of 1361W/m^2. The solar luminosity was about 30% lower in the Archean. The factor 4/3 is due to anisotropic solar heating on one side of the MM. The emissivity is taken to be unity, assuming a black-body approximation for the MM surface, and Öpik (1959) finds relatively low albedos of stony meteorites in the range 0.27-0.62. The heat capacity and density values are discussed in the next section.

The mass loss, or loss of radius due to sublimation (if it occurs) is given in terms of the Langmuir-Hertz formula and the saturation vapor pressure p_v, and for spherical grains Krivov et al. (1998) find

$$\frac{\partial r_p}{\partial t} = -C_e\frac{p_v}{\rho_p}\sqrt{\frac{M}{T}} \tag{3}$$

where $C_e = 4.377\times10^{-3}$ is the Langmuir constant of evaporation,

$$C_e = \sqrt{\frac{m_u}{2\pi k_B}}, \tag{4}$$

and M is the mean molecular weight relative to one atomic mass unit $m_u = 1.66\times10^{-27}$ kg. The vapor pressure model with its potential sources of error are discussed in more detail in the Appendix.

It is noted that (2) is valid up to the melting point, where the latent heat of solidification would act as a heat sink to maintain the melting temperature. We are not concerned with melting in this work. Furthermore, the "cold cases" we studied did not display any significant mass loss, as governed by (3).

2.2. Geocentric velocity, grain density and grain size

Most interplanetary dust and grains originate from comets and asteroids. The realization of multi-aerobraking scenarios are inherently very sensitive to the orbital elements of the incoming MM relative to the Earth. Based on Flynn (1989b), Jackson and Zook (1992), representative geocentric velocities are about 5 km/s for asteroidal grains and about 15 km/s for cometary grains for eccentric orbits with perihelia less than 1 AU. The computations of Jackson and Zook (1992) indicate a variation of the velocity distribution with grain size due to radiation pressure, Poynting-Robertson (PR) drag, and solar wind. The orbits of

particles in the size range from 5 to 50 μm in diameter are significantly perturbed by solar radiation (Flynn et al., 2008), and the PR drag force causes a 10 μm IDP to spiral towards the Sun, and a particle starting in the asteroid belt reaches 1 AU in 20,000 to 100,000 years (Flynn, 1989a). Particles produced by collisions in the Kuiper Belt spiral into the Sun on a time-scale short compared to the age of the Solar System.

The mean orbital velocity of the Earth is 29.78 km/s and influences the relative (geocentric) velocity, and hence high inclination cometary orbits (including retrograde motion) increases the geocentric velocity up to high values near 70 km/s (Hughes and Williams, 2000). The change of potential energy from large distance and to the upper atmosphere of the Earth adds to the kinetic energy, corresponding to an additional 11.2 km/s (escape velocity) to the initial geocentric velocity. The rotational velocity of the Earth is a minor contribution with 0.46 km/s at the equator, and can be ignored to first approximation.

The grain material density (before heating) depends on porosity and mineral composition. Unmelted chondritic particles smaller than 15 μm collected in the stratosphere have densities ranging between 0.3 and 6.2 g/cm^3, averaging at 2.0 g/cm^3 (Love et al., 1994). The lower range of density values indicate porous, primitive, uncompacted parent bodies. The same study showed that chondritic spherules (melted particles) had densities near 3.4 g/cm^3. Genge (2017) adopted the same value for basaltic MM prior to melting, and Öpik (1951) adopted the same value for conditric asteroidal dust.

Cometary dust grains collected in the stratosphere have an average density of roughly 1.0 g/cm^3 (Joswiak et al., 2007), and are largely dominated by high internal porosities and anhydrous mineralogy. The asteroidal IDPs in the same study had much higher average density of 3.3 g/cm^3. The size and density of individual dust particles from comet 81P/Wild 2 collected by the Stardust spacecraft indicated porous particles with 0.35 ± 0.07 g/cm^3 and a bulk density of all particles of 0.49 ± 0.18 g/cm^3 (Niimi et al., 2012). For asteroidal grains, we adopt 3.4 g/cm^3, and 1.0 g/cm^3 for cometary grains.

The grain size have a broad range for both cometary and asteriodal grains. We consider grain diameters in the range 20–300 μm similar to earlier modeling efforts (Genge, 2017; Jackson and Zook, 1992; Flynn, 1989b). Dust particles from comet 81P/Wild 2 display sub-micron sizes to several hundred microns (Hörz et al., 2006) with the majority of grains at smaller sizes. This is consistent with dominance of small grains in the coma of C/1995 O1 Hale–Bopp and 1P/Halley (Lasue et al., 2009). We chose two populations to represent asteroidal grains and cometary grains (Table 1).

The heat capacity is in the range 100–1000 J/kg/K. For meteoritic stone Öpik used 895 J/kg/K and a material density of 3.4 g/cm^3. One would expect lower heat capacity, heat conduction and effective density for more porous grains. However, we will use the same heat capacity for all particles (895 J/kg/K), but vary the material density.

2.3. Initial conditions and determination of the entry corridor

Heliocentric trajectories are deflected towards the Earth by gravity and the total cross section for capture at infinite distance and in the absence of an atmosphere is Öpik (1951), Kortenkamp and Dermott (1998),

$$\sigma_{c,\infty} = \sigma_{Earth}\left(1 + \frac{v_e^2}{v_\infty^2}\right), \tag{5}$$

where σ_{Earth} is the cross section of the Earth, v_∞ is the geocentric velocity prior to acceleration by the Earth, and $v_e = 11.2$ km/s is the escape velocity. Lower velocities v_∞ may increase the cross section dramatically, and impact of asteroidal grains are more likely than cometary grains with higher geocentric velocity. However, the likelihood of grazing angle low temperature histories of asteroidal versus cometary grains requires a closer examination since this is largely determined by the evolution of the trajectory through the atmosphere.

It was chosen to define the initial condition for each trajectory calculation in terms of the impact parameter Δ [m] and the velocity v_0 [m/s] at a certain distance x_0 from the Earth center (Fig. 2). It was convenient to use the perigee point R_P in the absence of an atmosphere as the variable input parameter, with R_P slightly larger than the Earth radius corresponding to a grazing encounter with the atmosphere. R_P equal to the Earth radius guarantees a descent in any atmosphere and a sufficiently large value of R_P leads to a brief encounter with the atmosphere, but with the grain escaping the earth on a zero-energy parabolic orbit. This particular value corresponds to an impact parameter that defines the total cross section at infinity that incorporates all captured MM. R_P can be determined from conservation of angular momentum, giving

$$v_0 \Delta = v_P R_P, \tag{6}$$

in terms of the respective tangential velocities as shown in Fig. 2. The perigee velocity in vacuum is given by

$$v_P = \sqrt{v_\infty^2 + 2\mu/R_P} \tag{7}$$

in terms of the geocentric velocity v_∞. The corresponding impact parameter can be found for a chosen R_P,

$$\Delta(R_P) = R_P v_P / v_0 = R_P \sqrt{1 + 2\mu(1/R_P - 1/R_{init})/v_0^2}, \tag{8}$$

where R_{init} is the initial radius vector (Fig. 2), and the initial velocity is $v_0 = \sqrt{v_\infty^2 + 2\mu/R_{init}}$. It can be shown that (5) is recovered from (8) by setting $R_P = R_{Earth}$ and $\sigma_c = \pi\Delta^2$. Hence, (5) can be generalized to any distance from earth, but with σ_c shrinking closer to Earth as the trajectories focus on the Earth.

A family of trajectories were generated spanning from a simple descent trajectory, to multi-skip trajectories and to a hyperbolic bypass trajectory. For each v_∞, a set of impact parameters $\Delta \in [\Delta_{min}(R_{lower}), \Delta_{max}(R_{upper})]$ were generated using the limits $R_{lower} = R_{Earth} + z_L$ and $R_{upper} = R_{Earth} + z_U$ for R_P, adjusted by trial and error to obtain the desired set of trajectories. As R_{upper} is increased, lower heating occurs with atmospheric entry at higher altitudes. Further increase leads to multi-skip elliptical orbits that are gradually circularized for every pass through the atmosphere. These scenarios correspond to orbital energies less than zero (elliptical orbits), with energy lost to friction for each pass.

A certain Δ^*_{max} corresponds to a zero energy parabolic trajectory after contact with the atmosphere, and impact parameters less than this value corresponds to capture. Only a very small fraction of the grains inside the cross section $\sigma_c = \pi(\Delta^*_{max})^2$ enters the atmosphere with a low heating trajectory. This corresponds to a narrow outer band of the circular cross section σ_c, with area $\delta\sigma_c \simeq 2\pi\Delta^*_{max} D$ with $D = \Delta^*_{max} - \Delta_{min}$. The relative area

$$\delta\sigma_c/\sigma_c = 2D/\Delta^*_{max} \tag{9}$$

is the fraction of particles, or the probability of entering in the narrow band D. This fractional area can be quite small; only on the order of 0.3% of all grains experience at least one grazing incidence (Genge et al., 1996). It can be shown that the relative area is independent of the evaluation distance from Earth, x_0. The absolute cross section evaluated at large (infinite) distance from the Earth is

$$\delta\sigma_{c,\infty} = \delta\sigma_c\left(1 + \frac{2\mu}{R_{init} v_\infty^2}\right), \tag{10}$$

and the total mass accumulated per time unit depends on atmospheric structure, material density, initial diameter and the distribution of geocentric velocities. The total number of grazing angle particles entering the Earths atmosphere per time unit can be expressed as

$$dN/dt = \int_0^\infty \int_0^\infty n_p(v, r_p)\delta\sigma_{c,\infty}(v, r_p) v dv dr_p, \tag{11}$$

where the integral runs over all geocentric velocities (here $v = v_\infty$ for notational simplicity), and $n_p(v, r_p)$ is the number density distribution

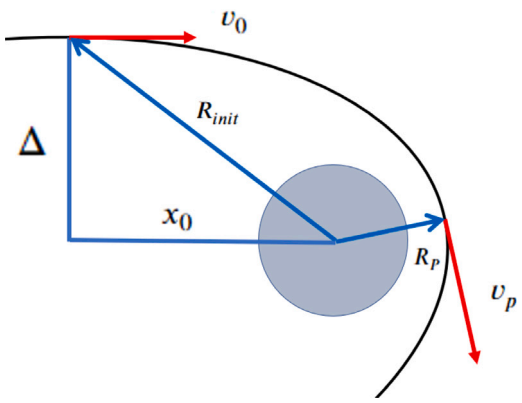

Fig. 2. Definition of the impact parameter Δ, the initial velocity v_0, and the position x_0 at some distance from Earth from which the calculations are started. The red vectors are perpendicular to the radius vector R_P and the line corresponding to Δ. With no atmospheric friction, the impact parameter can be found from a specification of R_P using energy and angular momentum conservation. (For interpretation of the references to color in this figure legend, the reader is referred to the web version of this article.)

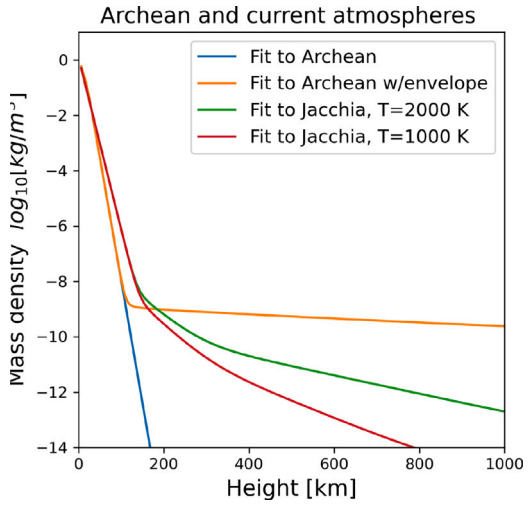

Fig. 3. Jacchia modern atmosphere for two different thermospheric temperatures and the Archean atmosphere with and without an extended H and He envelope. The envelope density is scaled down by a factor of 0.1 to account for mass loss up to 1 Ga after the sun settled on the main sequence at zero age (ZAMS). The density profiles are polynomial/exponential fits used in the trajectory simulations.

over velocity and size. The mass rate [kg/s] is obtained by replacing the number density distribution with the mass density distribution $\rho(v, r_p) = 4/3\pi r_p^3 \rho_p n_p(v, r_p)$.

3. Atmosphere models

The lower atmosphere in the Archean below 100 km altitude had a steeper density profile than the current atmosphere, due mainly to the heavier gas mixture with the larger fraction of CO_2 (Fig. 3), and a temperature that was comparable to the current lower atmospheric temperature. The upper atmosphere may have had a significant density from a remnant hydrogen/helium envelope from the protosolar nebula that had not yet dissipated fully after 1 Ga. This thin envelope could be more dense than the current thermospheric/exospheric density by two orders of magnitude or more, depending on height. The current thermospheric density and temperature varies with geomagnetic and solar activity, and can thus increase the capture rate of small MM with higher temperature and density. The main differences between the Archean and the Quaternary (current) atmospheric density profile is that the current atmosphere has a larger density scale height of the lower atmosphere (less steep gradient), but a more dilute upper atmosphere (the thermosphere) with a more steep density profile as shown in (Fig. 3). These differences create different temperature histories along the trajectories, given the same initial velocity and position of the MM.

3.1. The modern atmosphere, including the thermosphere

For the current atmosphere we used the semi-empirical Jacchia-77 model (Jacchia, 1977) that has been used to predict satellite drag, and which incorporates the thermosphere as well as the stratosphere and mesosphere. The atmospheric density is dominated by nitrogen in the lower layers, by mono-atomic oxygen in the lower thermosphere due to photodissociation of O_2, and by helium in the upper thermosphere. Hydrogen only has a small contribution. The gas density and temperature in the thermosphere is sensitive to solar irradiation, and geomagnetic activity. The global average temperature is about 1000 K (Emmert et al., 2021), and for high geomagnetic activity levels, it can reach 2000 K at higher geographic latitudes larger than 30 degrees (Jacchia, 1977). We chose 1000 K and 2000 K for the trajectory calculations.

For numerical purposes, one can interpolate in the Jacchia model mass density to any height along the MM trajectory. However, a more computationally efficient approach (speed is important due to the large number of evaluations along the trajectory) is to fit the density profile to a limited number of exponentials with different scale heights and reference densities,

$$\rho_a(z) = \rho_0 e^{-z/H_{lower}} + \sum_i \rho_i e^{-z/H_i}, \tag{12}$$

where the sum represents the fit to the thermosphere, while the first exponential represents an approximation to the lower atmosphere. This expression is evaluated every time step without interpolation (Fig. 3).

3.2. Archean atmosphere with extended hydrogen and helium exosphere

The composition of the Archean atmosphere is the most interesting in the context of MM supplying carbon compounds before life emerged. There is consensus in the literature that CO_2 and N_2 were the main constituents in the lower atmosphere (e.g., Catling and Zahnle, 2020; Kasting, 2014). Hydrogen was also contributing with larger number density and larger scale height than CO_2 from about 30 km above the homopause (Zahnle et al., 2019). The hydrogen mixing ratio was between 10^{-4} to 10^{-3} below 100 km altitude (Kasting, 2014).

The density profile in the lower atmosphere was generated using a 1D radiative-convective model with in the Platform for Atmosphere, Land, Earth and Ocean (PALEO, https://github.com/PALEOtoolkit) modeling framework (Eager-Nash et al. in preparation). The model atmosphere extends to 80 km with a composition of N_2, 10% CO_2 and 0.18% CH_4, using values from Catling and Zahnle (2020) for the beginning of the Archean, with a surface pressure of 1 bar. Radiative transfer was calculated using the Suite Of Community RAdiative Transfer codes (SOCRATES), based on Edwards and Slingo (1996) and Manners et al. (2017), with a convective adjustment based on Manabe and Strickler (1964), with a pseudoadiabatic lapse rate. Tropospheric water vapor decreases with pressure (Manabe and Wetherald, 1967) with a prescribed surface relative humidity of 0.7. Above the tropopause, the water vapor mixing ratio is fixed at the tropopause value. A Solar constant of 75% of the modern value is used based on Gough (1981).

The content of hydrogen and helium in the exosphere out to several Earth radii is highly uncertain. Despite thermal escape over time, it is reasonable to assume that the old exosphere had elevated density levels of hydrogen and helium, and could therefore collect more dust due to a larger effective cross section. Recent exoplanet data show low-mass planets possessing hydrogen dominated atmospheres accreted from the protoplanetary disk. This proto-atmosphere is potentially lost

at a rate that depends on the XUV luminosity of the young Sun, its rotation rate and initial amount of accreted hydrogen. If the Sun was a "rapid rotator", most of the hydrogen atmosphere could be removed in about 400 million years, but for the "slow rotator" sceanrio with lower XUV flux, 70% of the hydrogen atmosphere could remain at 1 Ga after accretion from the proto-planetary disk was completed (Johnstone et al., 2015).

Lammer et al. (2014) calculated the loss rates of hydrogen due to the soft X-ray and extreme ultraviolet (XUV) flux of the young Sun/star. It was found that 'sub-Earth' and Earth-mass planets can lose their captured hydrogen envelopes by thermal escape during the first 100 Myr after the protoplanetary disk dissipated. However, if the protosolar nebula was sufficiently depleted of dust and the protoplanetary luminosity was sufficiently low, it is possible that even Earth-mass planets would keep their hydrogen envelopes for a much longer time. Dust grains decouple dynamically from the gas and fall towards the protoplanetary surface, reducing the dust contents and opacity of the nebula so that the gas temperature and mass loss rate are reduced. Temperature-, density profiles, and outflow velocities in hydrogen envelopes that were exposed to 100 times higher XUV fluxes relative to the current solar value were calculated by Lammer et al. (2014). This corresponds to the situation 0.1 Ga after accretion was completed. For an Earth-mass planet at 1 AU from the early Sun, the hydrogen number density varied from about 4×10^{12} cm^{-3} at the base of the thermosphere at a radius $R_0 = 1.15 \times R_{Earth}$, to about 10^7 cm^{-3} at about 10 R_0 (their Fig. 4). Most of the hydrogen was dissociated into atomic hydrogen by XUV and EUV radiation.

We adopted the density profile of Lammer et al. (2014), and scaled down this profile by a factor of 0.1 to account for a 90% mass loss over 1 Ga, up until the early Archean. This large reduction is within the reported model variations and it is adopted to not overestimate the effect of the envelope. The scaled hydrogen (H) density at the homopause is then about 4×10^{11} cm^{-3}. Some of the hydrogen should have associated into H_2 by 1 Ga, when the solar XUV flux had diminished to about 5-10 times the current value. A number density of 2×10^{11} cm^{-3} corresponds to complete association. Zahnle et al. (2019) discussed the hydrogen escape rates with constraints based on the current Xenon concentrations, and hydrogen was now assumed to derive mostly from water, and not from accretion of gases from the protosolar nebula. The H_2 number density at the homopause in their nominal model with 20 times elevated XUV+FUV flux representing the early Archean, was around 10^{11} cm^{-3}, which is consistent with the hydrogen contents in the scaled down model we adopt.

The full Archean total mass density profile (lower atmosphere and upper hydrogen envelope) including the primordial fraction of helium relative to hydrogen, was fitted with an exponential-algebraic function of the form (12), and as shown in Fig. 3. A smooth transition was provided between the density profile for the lower atmosphere and the envelope density, at about 150 km altitude. This is obviously a crude modeling approach, but it suffices to demonstrate the differences in the capture rates of "cold" MM between Archean atmospheres with and without a dilute envelope.

4. Results

A number of velocity values v_∞ were chosen according to Table 1 and 15-30 trajectories in the range $[\Delta_{min}, \Delta_{max}]$ were calculated (in each atmosphere) for each population of given diameter, velocity and material density. The range of impact parameters was such that $R_{upper} - R_{lower}$ was typically less than 100 km. A total of 1260 trajectories were calculated to cover all cases in Table 1. The number of timesteps for each trajectory was between 60 000 and 180 000, to obtain the needed accuracy and numerical stability, and to follow the MM until descent to the surface. The maximum temperature along the trajectories was recorded. Fig. 4 shows a few trajectories of 100 μm cometary and asteroidal grains in the modern atmosphere, and the same color marks the trajectory of a single MM trajectory with specified initial conditions. All trajectories come in at the upper left in the figure. Some MM are captured and some bypass the Earth on a hyperbola if the contact with the atmosphere was at too large altitude.

4.1. Temperature histories

The temperature history as function of time is very intermittent with sharp "spikes" when the MM trajectory crosses the atmosphere. It is better to plot the temperature as function of velocity to compare the trajectories. This also reveals the multi-skip character of the orbits. Fig. 5 shows two examples of the trajectories of cometary and asteroidal grains in the average modern atmosphere. The trajectories start with low temperature set by solar radiation (lower right in the figure), and then the velocity increases until the atmospheric friction starts to act. The temperature increases to several hundred degrees. It decreases again as the velocity is reduced by friction (paths in the counter-clockwise direction). The grain can either escape, reaching the original temperature, or re-enter the atmosphere again, producing one or more heating events with successively lower velocity.

The maximum temperature is reached during the first pass, or in a subsequent pass, depending on initial velocity, diameter, and material density. The left panel in Fig. 5 for cometary grains shows that the highest temperatures are reached at first contact, followed by a direct descent. As the impact parameter increases, the maximum temperature at first contact decreases, and the MM returns for a second contact with a second temperature maximum (e.g., blue line). As the impact parameter is increased further, a temperature maximum is reached at first pass (here, around 600 °C) but the MM leaves the Earth on a hyperbolic trajectory (orange, green, red and violet paths).

For the asteroid grain example shown in Fig. 5, right panel, it is seen that the maximum temperature may occur in the final descent phase after several aerobraking events, rather than at first contact. For example, the trajectory marked with a turquoise line show two encounters with the atmosphere, before the final descent where maximum temperature is reached at about 350 °C.

4.2. Statistics of peak temperatures

The maximum temperature was recorded for each trajectory that led to descent to the surface of the Earth. These maximum temperatures are plotted as a function of fractional cross section in Figs. 6 and 7. The fractional cross section a_i is the relative cross section of an annulus with outer radius Δ^*_{max} and inner radius Δ_i,

$$a_i = 2(\Delta^*_{max} - \Delta_i)/\Delta^*_{max}, \tag{13}$$

where Δ_i is the smaller impact parameter and Δ^*_{max} is the maximum impact parameter that leads to capture. The total cross section of all captured MM is given by $\pi(\Delta^*_{max})^2$. A lower value of the impact parameter Δ_i corresponds to a larger cross sectional area of the annulus and a higher value of a_i.

The maximum temperature over all trajectories with impact parameters in the range $[\Delta_i, \Delta^*_{max}]$ usually occurs for Δ_i that corresponds to entry into the deepest layers of the atmosphere at first impact. Hence, trajectories entering in the fractional cross section a_i corresponds to heating below the temperature $T_{max}(\Delta_i)$. In other terms, the probability of heating below $T_{max}(\Delta_i)$ is equal to the fractional cross section a_i. The incoming mass flux to the top of the atmosphere for a certain grain population (of a given grain size and geocentric velocity) can then be scaled with this probability to obtain the corresponding mass flux to the surface.

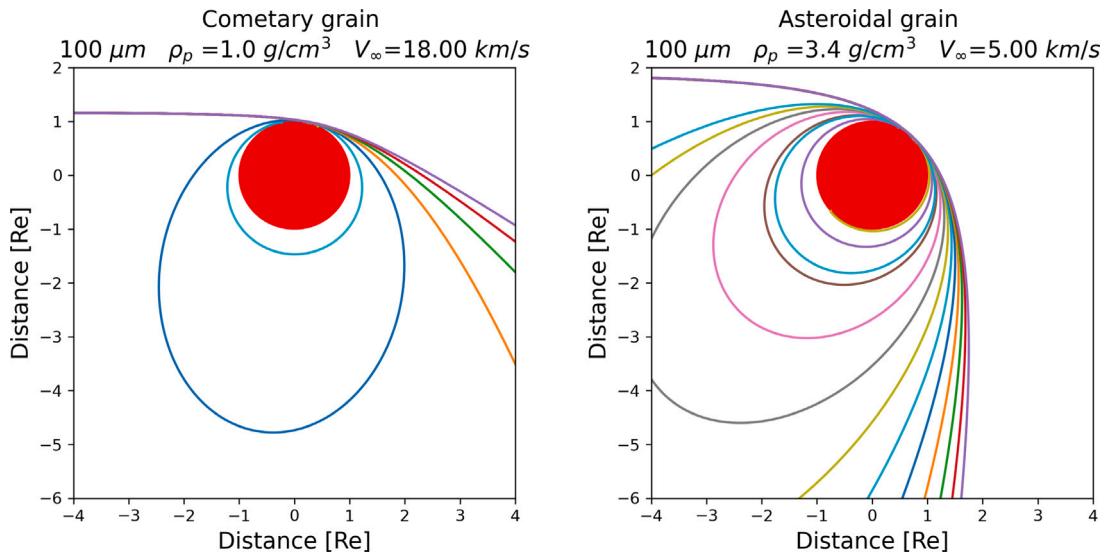

Fig. 4. Orbits of 100 μm MM grains in the modern (Quaternary) atmosphere. Left: cometary grain, Right: asteroidal grain. The thermospheric temperature was set to 1000 K, representing the average temperature. The incoming section of the MM orbit (top left) is generally hyperbolic relative to the Earth, and the variation of the impact parameter in the incoming trajectory is very slight (and invisible in the plots). For capture to occur, the orbit must become elliptical after the first encounter with the atmosphere. Each trajectory is marked with a unique color, here displaying one- or two-skip orbits. Some trajectories remain hyperbolic with lowered energy and the MM escapes the Earth after being slightly heated. The distance is in units of Earth radii.

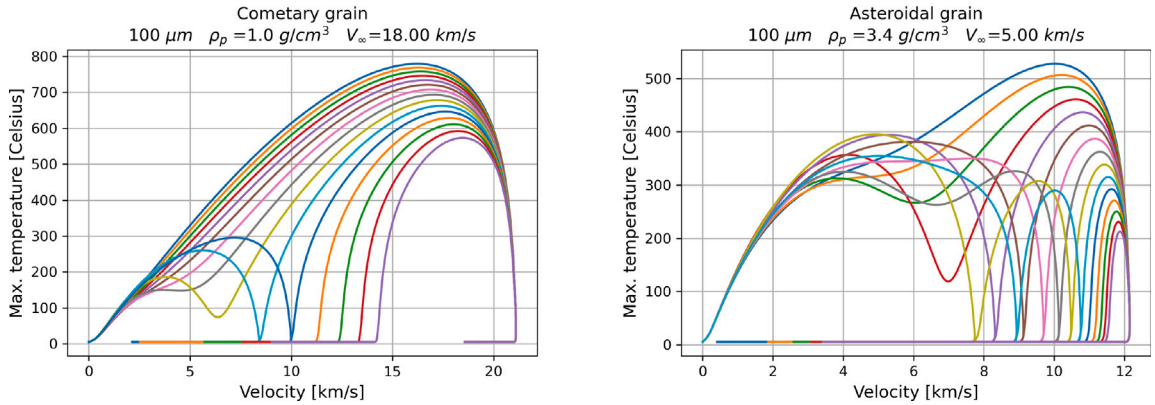

Fig. 5. Examples of velocity–temperature histories, corresponding to Fig. 4, and using the same color coding. *Left: Cometary grain.* Atmospheric entry at the highest altitudes generates one-skip trajectories (blue and turquoise) with highest temperature (about 650 °C) in the first pass, and 250–300 °C in the second pass. Lower entry altitudes generates direct descent with higher temperatures above 700 °C. *Right: Asteroidal grain* with two-skip trajectories (e.g., turquoise, light green and gray), now with the last descent phase giving the higher temperature in some cases. Again, lower entry altitudes generates direct descent (blue) with higher temperatures, here above 500 °C. (For interpretation of the references to color in this figure legend, the reader is referred to the web version of this article.)

Cometary grains. All the results for cometary grains are shown in Fig. 6. Most cometary grains experienced the highest temperature in the first pass due to their relatively high geocentric velocities, and the maximum temperature curves were monotonically increasing as function of increasing fractional cross section, as the MM entered at lower altitudes. There is typically a linear trend in the curves (exponentially increasing on the log-plots), and then a logarithmic trend (linear on the log-plot) for the higher maximum temperatures.

The smaller grains at 20 μm may have experienced surprisingly low maximum temperatures from below 200 °C in the modern atmosphere (upper row). The cross sectional fractions, or capture probability, was 1%–4% for maximum temperatures below 500 °C for the 20 μm grains, depending on geocentric velocity. For 100 μm grains, only the lowest velocity of 12 km/s produced temperatures below 500 °C. The thermospheric density is higher for higher thermospheric temperature, but this had a relatively small effect (by comparison of the left and right panels in the upper row). The reason for this is that the thermospheric friction does not produce a large reduction of orbital energy during the small number of orbits in the dilute thermosphere, and the main heating occurs in the lower atmosphere. There was however a small shift of the curves to lower maximum temperatures for higher thermospheric temperature due to increased mass density and friction in the thermosphere.

For the Archean atmosphere without an envelope (lower left panel), the cometary particles descended mostly in a direct trajectory as for the current atmosphere, but the maximum temperatures were overall larger. This is because the Archean lower atmosphere has a smaller density scale height than the modern one, and the frictional heating occurred over a smaller time interval.

The situation is different with an envelope (lower right panel). First, the grains decelerated in the extended envelope at quite low temperature (Fig. 8), and then they descended at a higher temperature in the lower atmosphere. Here, the smallest cometary grains maintained a low temperature around 300 °C for the smaller a_i (the larger impact parameters). For higher a_i, the grains performed a direct descent and the maximum temperature increased monotonically with smaller impact parameter. The curves in lower left panel in Fig. 6 are then not monotonically increasing, and typically there is a temperature plateau

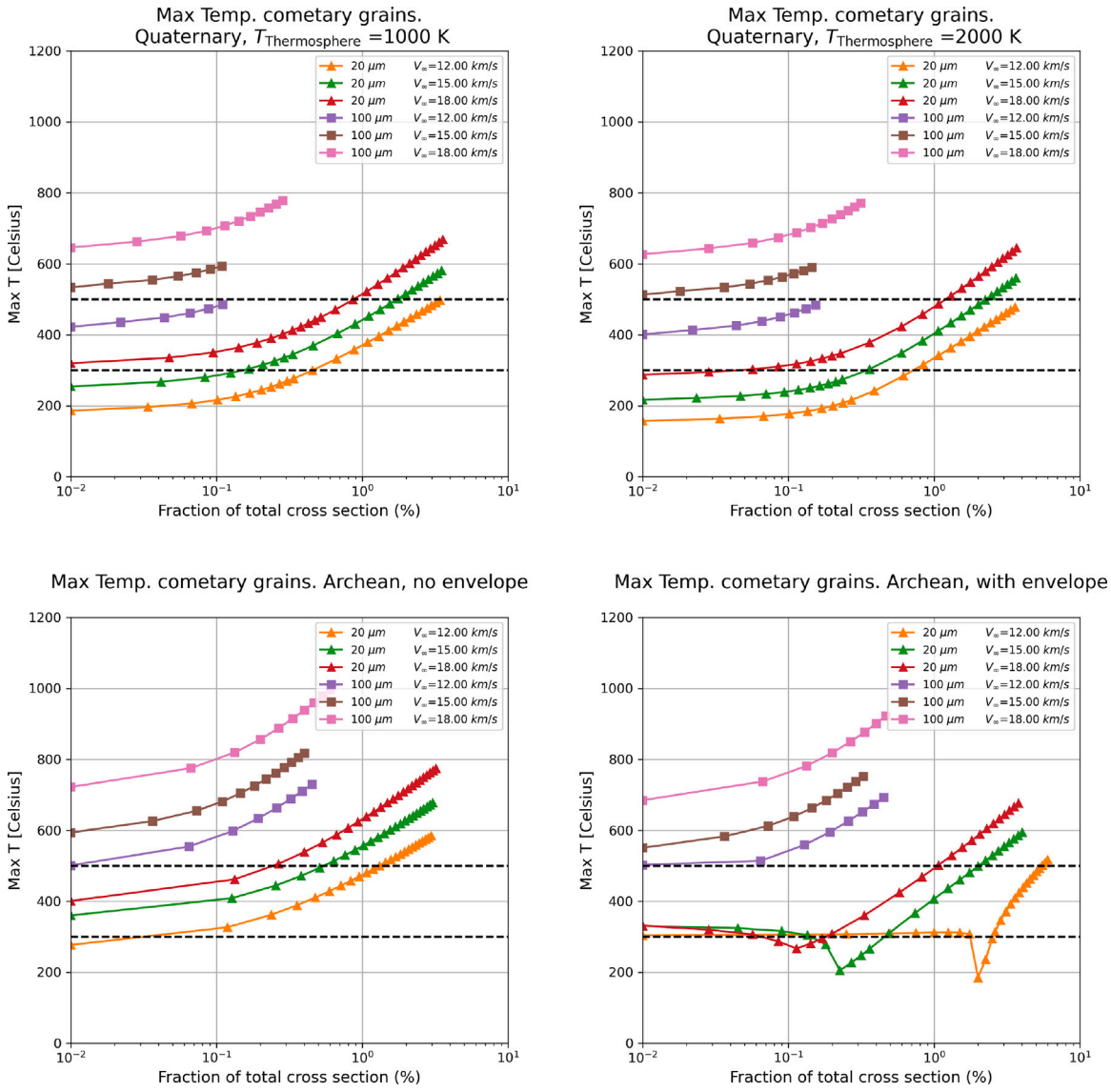

Fig. 6. Cometary grains in different atmospheres. Average modern atmosphere with a thermospheric temperature of 1000 K (upper left) and 2000 K (upper right). Archean without envelope (lower left), and with envelope (lower right). The first point to the left on all curves are for zero area (corresponding to $\Delta_i = \Delta^*_{max}$) is arbitrarily set to a small value of 0.01, to comply to the log-plot.

due to heating in the final descent phase (the smaller a_i), and then a monotonically increasing maximum temperature for direct descent trajectories. The temperatures stayed below 500 °C for fractional cross sections up to 1%–6%, depending on geocentric velocity between 18 and 12 km/s. The area fractions were lower and below 1.5% if the Archean had no envelope (lower left panel). Hence, there is a factor of 5-6 increase of the capture rate of these low temperature MM if an Archean envelope was present. However, it must be noted that the cross sectional fractions for heating below 500 °C in the Archean atmosphere with envelope are comparable to the fractions in the modern atmosphere (upper right, versus lower right panels).

None of the 100 μm cometary grains stayed below 500 °C for the Archean atmosphere, in contrast to the modern atmosphere. The reason for this is that the larger grains are less affected by friction if an envelope was present, and the grains are heated mainly in the lower atmosphere. The scale height is smaller there than for the modern atmosphere, and hence the heating pulse has a shorter duration with higher temperature to dissipate the same amount of kinetic energy.

Asteroidal grains. The asteroidal grains (Fig. 7) have smaller geocentric velocity than the cometary grains (on the average), resulting in more complex trajectories and multiple aerobraking events with temperature maxima that could occur in the final descent phase, (as shown in the right panel in Fig. 5). Again the curves display a temperature plateau from heating in the final descent phase, and then a monotonically increasing maximum temperature due to direct descent heating.

All the 300 μm asteroidal grains were heated to above 500 °C, regardless of the type of atmosphere. These grains are unmelted, but the temperature is high enough to break down any amino acids. The 100 μm grains stayed below 500 °C for cross sectional fractions below 0.3% for the modern atmosphere (upper row). Again, there was not a dramatic difference with variation of the thermospheric temperature. The cross sectional area for the same temperature limit was below 0.2% for the 100 μm grains in the Archean without an atmospheric envelope, but nearly all 100 μm grains were heated above 500 °C, with an envelope. It is surprising that 300 and 100 μm grains were heated to higher temperatures with an envelope added (lower left vs lower right panels). This is because the envelope decelerates the 100 and 300 μm grains so that the lower atmosphere is entered at a steeper angle.

In contrast, the 20 μm grains could be heated to very low maximum temperatures with relatively high probability with an Archean

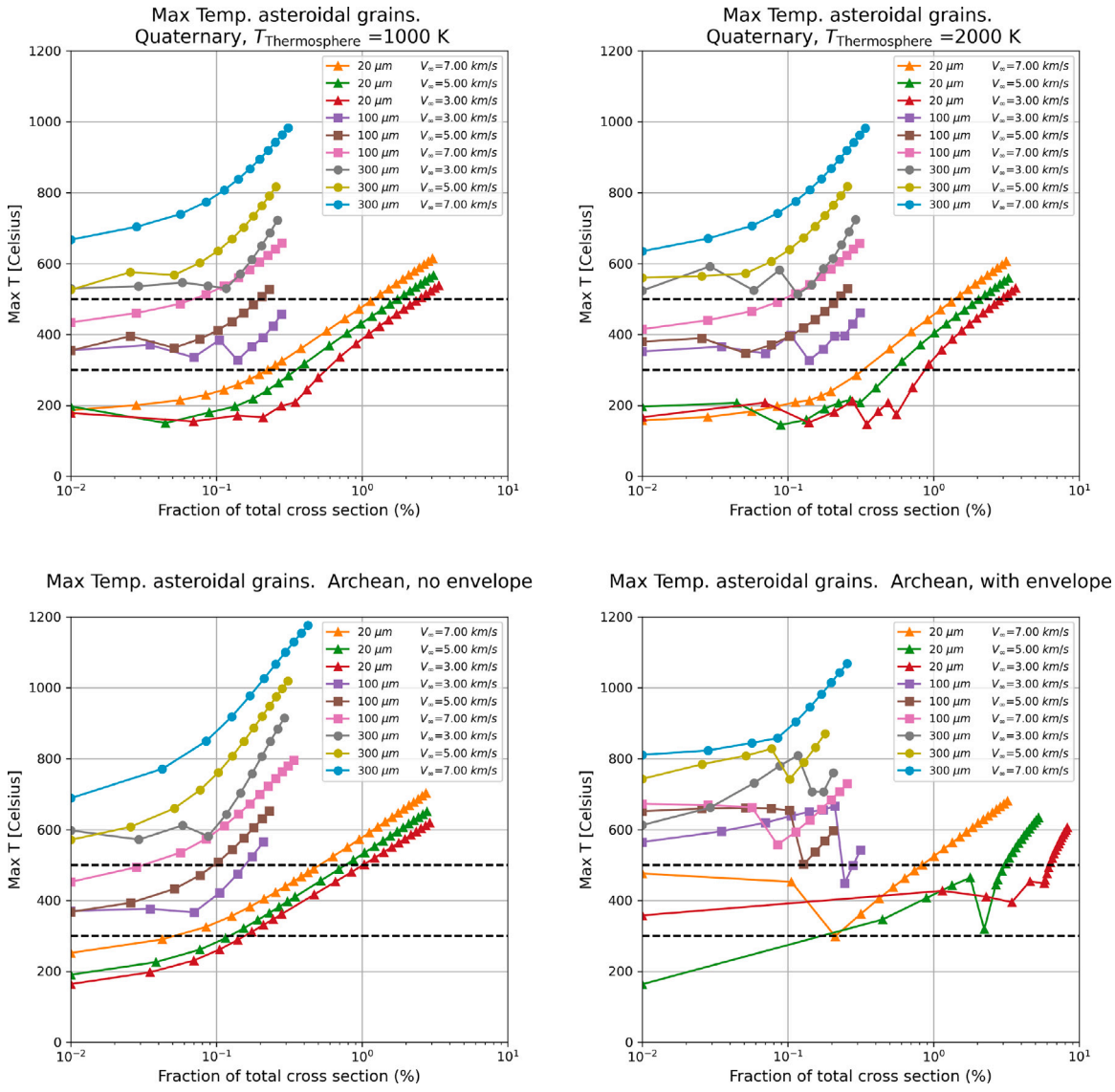

Fig. 7. Asteroidal grains in different atmospheres. Average modern atmosphere with a thermospheric temperature of 1000 K (upper left) and 2000 K (upper right). Acrhean without envelope (lower left), and with envelope (lower right).

envelope. The probability for temperatures below 500 °C was 7%–8% (lower right) for the 3 km/s case, and this was the largest relative cross section of all cases studied. Many of these trajectories correspond to the multi-skip variety with the mentioned "temperature plateau", where the deceleration in the envelope is important. The probability was about 1% without an envelope (lower left, red line), where most trajectories corresponded to direct descent.

The 20 μm grains could also experience very low maximum temperatures between 150 and 200 °C in the modern atmosphere, up to probabilities of 0.6% depending on thermospheric temperature. This will indeed preserve the amino acids, but then with relatively low probability. For the same grains, the temperatures stayed below 500 °C, with a probability below 3% for 3 km/s geocentric velocity, and about 1.5% for 7 km/s geocentric velocity.

5. Discussion

The current mass flux that will interact with the atmosphere is about 600 tons/year (6 $\times 10^5$ kg/year) in the mass range 10^{-7} to 10^{-8} g, corresponding to diameters of 10-20 μm (Flynn et al., 2004; Love and Brownlee, 1993). We found that the cross sectional area fractions corresponding to low temperature for these grains is 1%–4% in the modern atmosphere, depending on geocentric velocity. If we can assume an average probability of 2% over all velocities, only 12 tons/year of MM in this size range is heated to less than 500 °C. This is significantly less than the estimate of Flynn et al. (2004) of about 70 tons per year in the same size range and for temperatures below 600 °C. The total organic content is at least 3%–4% according to Flynn et al. (2004). This implies only about 0.5 tons of preserved organics per year, carried by of 10-20 μm MMs through the current atmosphere. Anders (1989) estimated that only 6×10^{-3}g/cm^2 of intact organic carbon would accumulate in 10^8 yr (0.1 Ga) from small grains, at present rates.

The situation may have been more favorable in the Archean with capture probabilities up to 8% for small asteroidal grains provided that the atmosphere had an extended envelope. Elevated capture probability in combination with higher dust density by a factor of at least 100 after the late heavy bombardment would elevate the mass flux accordingly. It is still uncertain if the material would provide sufficient concentration of amino acids in water to be of significance to the formation of life. Pooling and sedimentation of this material could be possible over long periods of time, but it is uncertain if stable conditions would prevail long enough to accumulate sufficient material locally over the required

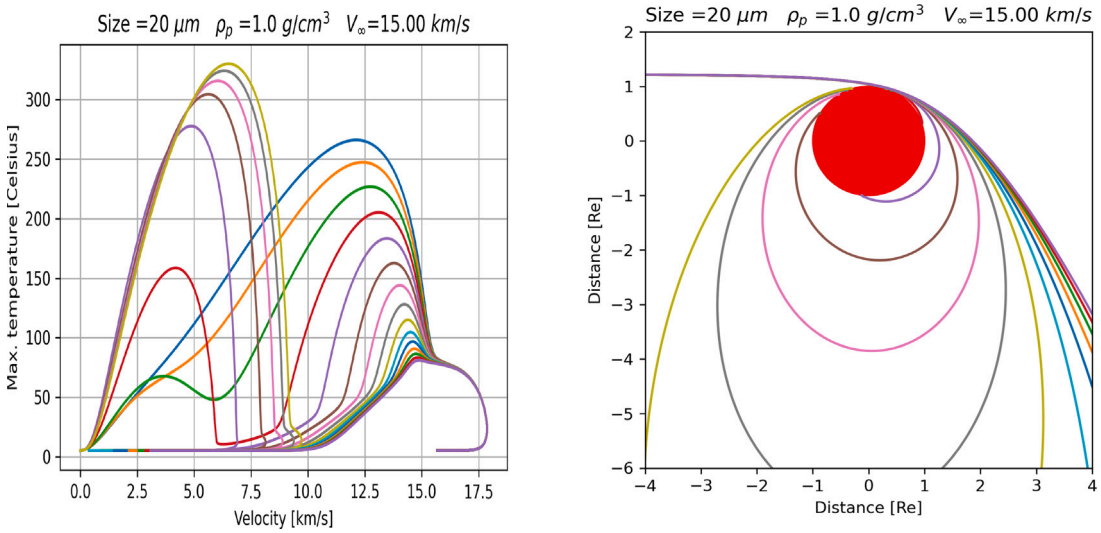

Fig. 8. 20 μm cometary grains with low heating in the Archean atmosphere with envelope. Left: Temperature histories. The blue and orange lines (near 250 °C maximum temperature) represent direct descent. Some orbits with smaller impact parameters and higher temperature are not shown. The violet track marks a transition to orbits with descent at second contact after coming back from an orbit around the Earth. The temperature plateau for the lower area fractions in the lower right panel in Fig. 6, corresponds to the group of orbits with max temperature of near 300 °C during second contact. Right: Corresponding orbits. (For interpretation of the references to color in this figure legend, the reader is referred to the web version of this article.)

timescales on the order of 10^8 yr. More research on local accumulation effects in the Archean would be needed to determine if sufficient concentrations of amino acids could be obtained for life synthesis. Three plausible mechanisms for further investigation are suggested. (1) Wind trapping is proven to concentrate MM in Antarctica after being released from ice, and 100 μm particles can be trapped in depressions or eddies behind rocks. Urban micrometeorites are also subject to wind trapping effects on flat roofs, with increased concentration along edges and in corners. (2) Ice trapping effects. Dust that falls on the Greenland ice for a few thousand years moves to the warm ice margin where it melts and leaves MM dust concentrated by many orders of magnitude. This is an efficient process that could have happened in the Archean, but also at the end of the Snowball Earth/Cryogenian era about 700-650 Myr ago. (3) Ocean current winnowing. MM particles on the ocean floor are much larger than the sub-micron clay particles that dominate deep ocean sediments, and ocean currents could have provided winnowing effects that made outcrops of MMs. This might have been prominent on an early Earth with reduced land mass.

We speculate that larger meteorites in the Archean were an equally probable transport mechanism, since they could deliver larger local surface concentrations of amino acids. Furthermore, impact in shallow seas offers a promising scenario that could limit the impact heating, while at the same time deliver higher concentrations of meteoritic material directly in water. On the other hand, larger meteorites or fragments thereof sink to the ocean floor where they may become covered with hydrated silicate sediment and become isolated with their relatively small area/mass ratios. Chyba et al. (1990) estimated that during the heavy bombardment of the inner solar system, that started about 4 Ga ago, the Earth could be accreting 10^6 to 10^7 kg/yr of intact organic material by comet impact if the Earth had a CO_2 atmosphere with 10 bar ground pressure. Only 1% of this material was taken to be amino acids, based on carbonacious chondrite abundances. Impact velocities in the ocean had to be low enough to permit organics to survive heating below 1800 K for less than a second (below about 9 km/s), and the dominating mass flux was due to 100-200 meter cometary objects. Most current models for Archean atmospheres have a much lower ground pressure around 1 bar, and the corresponding infall rate of intact amino acids was therefore probably lower due less friction and higher ground impact velocities. Chyba et al. (1990) found that comets or asteriods as small as 100 meters could not be aerobraked to impact velocities less than 10 km/s in a 1 bar CO_2 atmosphere. Infall of meteorites and smaller particles could therefore have been be the main source of intact amino acids in these lower density Archean atmospheres, rather than larger objects.

Organic compounds may also have accumulated on the primitive Earth via other mechanisms including atmospheric synthesis and deep-sea hydrothermal vent synthesis (Cleaves, 2012), and abiotic synthesis of amino acids in the oceanic lithosphere (Ménez et al., 2018). This raises the question of the relative significance of the various endogenous sources in comparison to exogenous delivery by meteorites and micro-meteorites.

The time frame for prebiotic chemistry is uncertain. There are indications of isotopically light carbon in 3.7 Ga sedimentary rocks (Rosing, 1999; Catling and Zahnle, 2020), and prebiotic chemistry relevant for life could therefore have occurred already in the Hadean (from solar system formation at 4.567 – 4.0 Ga), after a few 100 My after a Moon forming impact.

The origin of the proposed hydrogen envelope is highly uncertain. An alternative scenario would be a steady-state source–sink balance between tectonic degassing and hydrogen escape. Zahnle et al. (2019) discussed the associated hydrogen escape and constraints based on the current Xenon concentrations, and found an escape rate of 1.9×10^{14} mol H_2 yr^{-1} at the homopause, at 82% of the diffusion-limited flux, whereas higher H_2 atmospheres, including the cases considered by Lammer et al. (2014) and Johnstone et al. (2015), escapes by radiative heating (energy input from FUV/XUV photons vs. energy needed to lift hydrogen out of the potential well). The mass of a high H_2 atmosphere will (using a rough approximation to the numbers in Zahnle et al. (2019), Fig. 5, where S is XUV + FUV fluxes relative to the modern Sun) decrease linearly at $\sim 8 \times 10^{14}$ mol H_2 $(S/10)$ yr^{-1}, or 1 Earth ocean per 100 $(S/10)$ My, suggesting a short-lived transient H_2 envelope in this scenario, until a steady-state balanced by tectonic inputs is reached. It is also noted that impact degassing is a possible additional source of H_2 atmospheres (e.g., Schaefer and Fegley, 2010).

An important aspect is radiative degradation of amino acids in space over long time periods (Kobayashi et al., 2021), and shielding becomes ineffective in the X-ray range for sub-millimeter meteoritic grains. Once the grains are released from the parent body, they are exposed to radiation, and the probability of bond breaking in amino acids increases with time. Ions from the solar wind may also have contributed to degradation. Iglesias-Groth et al. (2011) found that the 20 proteinaceous amino acids can survive relatively large amounts of gamma radiation

doses of 14 MGy delivered by the decay of radionuclides during the lifetime of the Solar system, at a depth of 20 m or more of the parent object. The contribution from cosmic rays to this total dose is negligible at these depths because of shielding.

The analysis of Flynn et al. (2008) indicate that organic matter may still survive exposure to radiation in the inner Solar System for 20,000 to 100,000 years in particles as small as 10 μm. However, depending on energy, X-rays may have a characteristic penetration depth much larger than a micron, and hence small grains with diameter below 100 μm are subject to penetrating radiation, and the probability of bond breaking determines the survival probability of amino aids over a long time.

The solar X-ray and XUV flux in the Archean in the wavelength range 1-960 Å was about 5-10 times larger than the current value (Johnstone et al., 2015), or about 0.01 W/m^2 at 1AU. At 1 Å, or energies on the order of 10 keV, the penetration depth is about 100 μm in meteoritic material (Uesugi et al., 2010). For 30 Å or energies on the order of 400 eV, the penetration depth is about 0.1 μm, and would be insignificant for a 10 μm MM. Intermediate energies would be able to degrade amino acids in a large fraction of the volume of MM with diameters less than 100 μm, and Zubavichus et al. (2004) studied the decomposition of amino acids for soft X-rays up to about 500 eV.

The average irradiation in the Archean was in the range 10^{-4} to 10^{-3} W/m^2/nm in the X-ray to XUV range (Cnossen et al., 2007). This corresponds to about 5–50 interactions over the cross section of a 20 μm diameter MM, per second, per nm, near an X-ray photon energy of 10 keV, at 1 AU distance from the young Sun. If 1% of the volume was organic matter, it would be exposed to roughly 1-10 hard X-ray photons per second (and more for softer X-rays). The molar mass of amino acids is on the order of 100 g/mol, and if we can assume that 1 wt% of a 20 μm MM was amino acids, then 10^{-8} g or 6×10^{13} amino acid molecules would be exposed to 1-10 X-ray photons per second. Over 100 000 years, this would be $3\text{–}30 \times 10^{12}$ X-ray photons, comparable to the number of amino acid molecules in the same MM. Furthermore, variability of the early Sun in the form of flares would elevate both the X-ray and gamma ray fluxes to much higher levels, but over limited time intervals (a factor of 10 intensity increase for events lasting only a few hours for the current Sun). Possible amino acid degradation via ionization or oxidation effects subject to the X-ray flux in the Archean should be examined closely to determine if the these grains could preserve intact amino acids over timescales of at least 100 000 years after release by the parent object.

The maximum temperature of the MM's during the flight through the atmosphere depends on their heat capacity. The effective heat capacity per volume unit is lower for higher porosity, and so cometary grains may be heated to higher temperatures than solid chonditric material for the same size and frictional heat input. Hence, our temperature estimates are "best case scenarios" for the cometary grains, as we assumed the same heat capacity as for chonditric material. Likewise, the heat conduction coefficient is also uncertain for heterogeneous and porous material. However, the conduction timescale is probably short enough so that isothermal conditions is a reasonable assumption for the size range of MM we have studied, and "thermal shielding" of the interior would be inefficient. Further complications include situations where there are phase changes that include dehydration of phyllosilicates and sublimation of organics. These processes act as heat sinks before melting silicate components with the lowest melting point. Aerobraking trajectories minimize T_{max} but they also increase the heating duration that may influence the effect of heat sinks due to phase changes.

Aerobraking trajectories are sensitive to the density profile above 150 km, as shown by the varying results for the different atmospheric density profiles shown in Fig. 3. Small friction in higher atmospheric layers above 200 km at first pass may be enough to capture some MM in elliptical orbits for subsequent aerobraking to occur, thereby increasing the "cold capture" probability. The density profile of the current atmosphere is dependent on the thermospheric temperature that varies with solar activity. The solar activity level was higher and more variable in the Archean and the higher average X-tay flux was accounted for in the model for the hydrogen and helium envelope. Short-time variation of the solar flux was however not considered. Elevated densities and therefore larger cold capture probabilities than those calculated could have occured intermittently also in the Archean.

Of effects that could influence entry speeds of asteroidal grains and comet dust are circularization due to the Poynting Robertson (PR) effect and orbit perturbations due to Jupiter (Yang and Ishiguro, 2018). We implemented geocentric velocities from Jackson and Zook (1992) that accounted for radiation pressure, PR-drag and solar wind. Nesvorny et al. (2010) argued for relatively low atmospheric entry speeds of 100 μm JFC cometary and asteroidal grains with average values of 14.5 km/s, and 12.5 km/s respectively. For 200 μm diameter, the majority of JFC cometary grains and asteroidal grains had entry speeds in the 11.2–15 km/s range (implying near zero geocentric velocity at large distance from the Earth). The reason for the relatively low entry speeds in their model was PR drag which circularized the orbits before reaching the Earth. These estimates are lower than the values we implemented from Jackson and Zook (1992) (adding 11.2 km/s to the geocentric values in the values in Table 1.)

6. Conclusion

A numerical study was performed for MM with low entry heating in the modern (Quaternary) and Archean atmospheres. Cometary and asteroidal grains in the range 20–300 μm were considered, with geocentric velocities in the range 12–18 km/s for cometary grains and 3–7 km/s for asteroidal grains. The main result is that delivery of intact amino acids from space via small grains near 20 μm was possible in the Archean atmosphere with elevated probability for asteroidal grains or comparable probability for cometray grains, (relative to the Quaternary atmosphere) provided that the Archean atmosphere had a dilute hydrogen and helium exosphere. The capture probability for heating to less than 500 °C for asteroidal grains was about twice the value obtained for the Quaternary atmosphere, with a probability of about 8% for a geocentric velocity of 3 km/s, and lower probability for higher velocity. Smaller grains were more affected by the drag force in the envelope and the velocity was reduced more before entering the lower atmosphere, limiting the heating there. Small cometary grains of 20 μm could be heated to maximum temperatures below 500 °C with a probability of about 6% for a geocentric velocity of 12 km/s, and lower probability for higher velocity. If the Archean atmosphere did not have a remnant envelope, these probabilities were below 1.5%, less than for the Quaternary atmosphere.

The Jacchia-77 model (normally applied to calculate the effects of satellite drag) was used for the modern (Quaternary) atmosphere, and the thermospheric temperature was varied from average to elevated values during higher solar and geomagnetic activity. Increased thermospheric temperature corresponds to higher thermospheric density and larger drag. Increased temperature and density in the thermosphere lowered the maximum temperatures of the MM only slightly. We found very low maximum temperatures in the range 150–200 °C, for 20 μm asteroidal and cometary grains in the Quaternary atmosphere for trajectories entering at the highest altitudes, but the capture probability in this temperature range was typically less than 0.3%. The 100 μm asteroidal grains were heated to less than 500 °C with probability of 0.3%. These values are consistent with Farley et al. (1997) which estimated that less than 1% of all MM are heated to less than 600 °C in the modern atmosphere.

It is important to note that larger grains have smaller probabilities of low heating in general, but their larger volume may compensate such that comparable amounts of intact amino acids could potentially be delivered from larger grains. However, there is a cutoff value where large grains will be heated to above pyrolysis temperature (corresponding to zero cold capture probbaility). For example, all the 100 μm cometary

grains were heated to above 500 °C for the Archean atmosphere. Hence, the exact amounts of intact amino acids delivered to the surface of the Earth depends on the grain size distribution weighed against the cold capture probabilities.

It is however too early to conclude with regards to the role of MM with respect to the origin of life on Earth. A closer look at radiative degradation in space of amino acids in small grains is encouraged, since the X-ray flux from the Sun in the early Archean was 5-10 times larger than it is today (e.g., Johnstone et al., 2015), and smaller grains with diameters below about 100 μm may not have provided efficient long-time shielding against radiation energies above a few hundred eV. Another bottle neck that needs further attention is that *local* accumulation of intact extraterrestrial amino acids from micrometeorites in water could have been insufficient in order to reach critical concentrations for life to form, both due to the limited influx rate and the need for environmental and geological stability so that local accumulations could be preserved for sufficiently long times.

CRediT authorship contribution statement

R. Skartlien: Numerical modeling of trajectories, Analysis of the results, Literature review, Writing the manuscript and coordination. **J.B. Kihle:** Imaging urban micrometeorites, Proofreading. **J. Larsen:** Collecting urban micrometeorites, Proofreading. **J.K. Eager-Nash:** Providing data, Modelling of the Archean atmosphere, Writing a section of the manuscript, Proofreading. **T.L. Palmer:** Ensured general initial conditions based on impact parameter and conservation of angular momentum, Arguments for X-ray irradiation and amino acid bond breaking, Proofreading, Data presentation, Figure alterations. **T.J. Boxer:** Modelling the Archean atmosphere. **S.J. Daines:** Modelling the Archean atmosphere, Discussion of envelope models for the Archean atmosphere and prebiotic life chemistry. **N.J. Mayne:** Modelling the Archean atmosphere, Proofreading.

Declaration of competing interest

There is no conflict of interest.

Data availability

Data will be made available on request.

Acknowledgments

The authors wish to acknowledge the constructive feedback from the reviewers, who also provided additional material. This project was financed by IFE through basic research funds, with the initiatives of K. Hald, J. K. Sveen and L. Patruno. K. Knudsen contributed with arguments on gas accumulation during atmospheric entry. O. Skjaeraasen raised the issue of X-ray irradiation of cosmic grains. K. Furtado of Met Office initiated contact between IFE and the University of Exeter. J.K.E-N would like to thank the Hill Family Scholarship, supported by University of Exeter alumnus, and president of the University's US Foundation Graham Hill (Economic & Political Development, 1992) and other donors to the US Foundation. S.J.D thanks the John Templeton Foundation, United States Grant [62220]. N.J.M gratefully acknowledge funding from a Leverhulme Trust Research Project Grant [RPG-2020-82]. N.J.M was supported by a UKRI Future Leaders Fellowship [grant number MR/T040866/1]. Archean atmosphere data was produced using Met Office Software.

Appendix. Sublimation thermodynamics, vapor pressure, and a clarification

A generalized form for the sublimation rate (3) can be achieved by accounting for the fractal dimension of the grain (Krivov et al., 1998), resulting in a scaled evaporation constant C_e (the value in (4) represents the special case of a spherical grain). The saturation vapor pressure is in general (Krivov et al., 1998)

$$p_v = p_0 \exp\left(-\frac{M m_u L_v}{k_B T}\right) \equiv \exp\left(-\frac{B}{T} + A\right). \tag{14}$$

The latter traditional form is given in terms of the Antoine coefficients A and B, and we note that $p_0 = exp(A)$. The majority of stony meteorites are chondrites consisting of cemented granules of chondrules and we adopted A and B values for meteoritic stone as given by Öpik (1959). We could not find updated values in the literature, and most work on MM entry adopt these values.

There has been a fair amount of confusion in the literature regarding the use of different units for the pressure (SI or cgs) and type of logarithmic base (natural or base 10). The source of the problem is that the Antoine coefficient A must be supplied with this information, and this is rarely the case. If the units and logarithmic base are unspecified, the corresponding numerical value of the scaling factor p_0 remains arbitrary, which is obviously a potential source of grave error. The vapor pressure formula by Öpik (1959) is in terms of the base 10 logarithm and in dynes per square centimeter (cgs units),

$$log_{10}(p_v) = 10.6 - 13500/T \ (\mathrm{d/cm^2}, \mathrm{cgs}). \tag{15}$$

To convert from cgs units to SI, with 0.1 Pascals for 1 dyne/square centimeter, one obtains

$$log_{10}(p_v) = 10.6 - 1.0 \ (\mathrm{N/m^2}, SI) - 13500/T \ (\mathrm{N/m^2}, SI). \tag{16}$$

Genge (2017) used in fact A = 9.6, and B = 26700 based on a range of values given in Love and Brownlee (1991), but apparently the exponential form (or natural logarithm) was used rather than base 10.

To convert to the exponential form (14) in SI,

$$ln(p_v) = 2.3(10.6 - 1.0 - 13500/T) = 22.08 - 31050/T \tag{17}$$

using $e^{2.3} = 10$. The value B = 31050 K corresponds to a mean molecular weight of 42.7 using Öpiks value for the latent heat of L_v = 6.05e6J/kg, and Genge (2017) used a molecular weight of 45. We used this B-value and A = 22.08 in the exponential form (14) to generate the same vapor pressure as Öpik.

For amino acids, B is in the range 13-16000 K and A is in the range 31-37 ((Volkova et al., 2015), in SI and exp-form). However, the amino acids are embedded into the MM material and values for pure amino acid would probably produce too high vapor pressures and would not be representative for sublimation of amino acids from MM material. For pure carbon, $A = 36$ and L_v = 7.27e7 J/kg giving B = 104940 K, and for silicate, $A = 30$ and L_v = 7.12e6 J/kg giving B = 57383 K (Kimura et al., 1997) (both in SI and exp-form).

References

Anders, E., 1989. Pre-biotic organic matter from comets and asteroids. Nature 342 (6247), 255–257. http://dx.doi.org/10.1038/342255a0.

Bertrand, M., van der Gaast, S., Vilas, F., Hörz, F., Haynes, G., Chabin, A., Brack, A., Westall, F., 2009. The fate of amino acids during simulated meteoritic impact. Astrobiology 9 10, 943–951.

Canepa, C., 2013. The role of catalysis on the formation of an active proto-enzyme in the prebiotic aqueous environment. Nat. Sci. 5, 549–555. http://dx.doi.org/10.4236/ns.2013.55069.

Canepa, C., 2016. The role of autocatalysis on the chemical diversity of the prebiotic ocean of early Earth. Int. J. Astrobiol. 15 (1), 57–64. http://dx.doi.org/10.1017/S1473550415000099.

Canepa, C., 2020. A model study on the dynamics of the amino acid content in micrometeoroids during atmospheric entry. Chemistry 2 (4), 918–936. http://dx.doi.org/10.3390/chemistry2040058, URL https://www.mdpi.com/2624-8549/2/4/58.

Carrillo-Sánchez, J.D., Gómez-Martín, J.C., Bones, D.L., Nesvorný, D., Pokorný, P., Benna, M., Flynn, G.J., Plane, J.M., 2020. Cosmic dust fluxes in the atmospheres of earth, mars, and venus. Icarus 335, 113395. http://dx.doi.org/10.1016/j.icarus.2019.113395, URL https://www.sciencedirect.com/science/article/pii/S0019103519301824.

Carrillo-Sánchez, J.D., Nesvorný, D., Pokorný, P., Janches, D., Plane, J.M.C., 2016. Sources of cosmic dust in the earth's atmosphere. Geophys. Res. Lett. 43 (23), 11,979–11,986. http://dx.doi.org/10.1002/2016GL071697, arXiv:https://agupubs.onlinelibrary.wiley.com/doi/pdf/10.1002/2016GL071697, URL https://agupubs.onlinelibrary.wiley.com/doi/abs/10.1002/2016GL071697.

Catling, D.C., Zahnle, K.J., 2020. The Archean atmosphere. Sci. Adv. 6 (9), eaax1420. http://dx.doi.org/10.1126/sciadv.aax1420, arXiv:https://www.science.org/doi/pdf/10.1126/sciadv.aax1420, URL https://www.science.org/doi/abs/10.1126/sciadv.aax1420.

Chyba, C., Sagan, C., 1992. Endogenous production, exogenous delivery and impact-shock synthesis of organic molecules: An inventory for the origins of life. Nature 355 (6356), 125–132. http://dx.doi.org/10.1038/355125a0.

Chyba, C.F., Thomas, P.J., Brookshaw, L., Sagan, C., 1990. Cometary delivery of organic molecules to the early earth. Science 249 (4967), 366–373. http://dx.doi.org/10.1126/science.11538074, arXiv:https://www.science.org/doi/pdf/10.1126/science.11538074, URL https://www.science.org/doi/abs/10.1126/science.11538074.

Cleaves, H.J., 2012. Prebiotic chemistry: What we know, what we don't. Evol.: Educ. Outreach 5, 342–360.

Cleaves, H.J., Chalmers, J.H., Lazcano, A., Miller, S.L., Bada, J.L., 2008. A reassessment of prebiotic organic synthesis in neutral planetary atmospheres. Orig. Life Evol. Biospheres 38, 105–115.

Cnossen, I., Sanz-Forcada, J., Favata, F., Witasse, O., Zegers, T., Arnold, N.F., 2007. Habitat of early life: Solar X-ray and UV radiation at Earth's surface 4–3.5 billion years ago. J. Geophys. Res.: Planets 112 (E2), http://dx.doi.org/10.1029/2006JE002784, arXiv:https://agupubs.onlinelibrary.wiley.com/doi/pdf/10.1029/2006JE002784, URL https://agupubs.onlinelibrary.wiley.com/doi/abs/10.1029/2006JE002784.

Duprat, J., Engrand, C., Maurette, M., Kurat, G., Gounelle, M., Hammer, C., 2007. Micrometeorites from central antarctic snow: The CONCORDIA collection. Adv. Space Res. 39 (4), 605–611. http://dx.doi.org/10.1016/j.asr.2006.05.029, URL https://www.sciencedirect.com/science/article/pii/S0273117706004522.

Edwards, J.M., Slingo, A., 1996. Studies with a flexible new radiation code. I: Choosing a configuration for a large-scale model. Q. J. R. Meteorol. Soc. 122 (531), 689–719. http://dx.doi.org/10.1002/qj.49712253107, arXiv:https://rmets.onlinelibrary.wiley.com/doi/pdf/10.1002/qj.49712253107, URL https://rmets.onlinelibrary.wiley.com/doi/abs/10.1002/qj.49712253107.

Emmert, J.T., Drob, D.P., Picone, J.M., Siskind, D.E., Jones Jr., M., Mlynczak, M.G., Bernath, P.F., Chu, X., Doornbos, E., Funke, B., Goncharenko, L.P., Hervig, M.E., Schwartz, M.J., Sheese, P.E., Vargas, F., Williams, B.P., Yuan, T., 2021. NRLMSIS 2.0: A whole-atmosphere empirical model of temperature and neutral species densities. Earth Space Sci. 8 (3), http://dx.doi.org/10.1029/2020EA001321, arXiv:https://agupubs.onlinelibrary.wiley.com/doi/pdf/10.1029/2020EA001321, URL https://agupubs.onlinelibrary.wiley.com/doi/abs/10.1029/2020EA001321, e2020EA001321 2020EA001321.

Engrand, C., Maurette, M., 1998. Carbonaceous micrometeorites from Antarctica. Meteorit. Planet. Sci. 33 (4), 565–580. http://dx.doi.org/10.1111/j.1945-5100.1998.tb01665.x, arXiv:https://onlinelibrary.wiley.com/doi/pdf/10.1111/j.1945-5100.1998.tb01665.x, URL https://onlinelibrary.wiley.com/doi/abs/10.1111/j.1945-5100.1998.tb01665.x.

Farley, K.A., Love, S.G., Patterson, D.B., 1997. Atmospheric entry heating and helium retentivity of interplanetary dust particles. Geochim. Cosmochim. Acta 61, 2309–2316.

Flynn, G.J., 1989a. Atmospheric entry heating: A criterion to distinguish between asteroidal and cometary sources of interplanetary dust. Icarus 77 (2), 287–310. http://dx.doi.org/10.1016/0019-1035(89)90091-2.

Flynn, G.J., 1989b. Atmospheric entry heating of micrometeorites. In: Lunar and Planetary Science Conference Proceedings. Vol. 19, pp. 673–682.

Flynn, G., Keller, L., Jacobsen, C., Wirick, S., 2004. An assessment of the amount and types of organic matter contributed to the Earth by interplanetary dust. Adv. Space Res. 33 (1), 57–66. http://dx.doi.org/10.1016/j.asr.2003.09.036, URL https://www.sciencedirect.com/science/article/pii/S0273117703008548, Space Life Sciences: Steps Toward Origin(s) of Life.

Flynn, G.J., Keller, L.P., Wirick, S., Jacobsen, C., 2008. Organic matter in interplanetary dust particles. In: Proceedings of the International Astronomical Union. Vol. 4, pp. 267–276.

Folco, L., Cordier, C., 2015. Micrometeorites. In: Planetary Mineralogy. European Mineralogical Union, http://dx.doi.org/10.1180/EMU-notes.15.9.

Genge, M.J., 2017. The entry heating and abundances of basaltic micrometeorites. Meteorit. Planet. Sci. 52 (5), 1000–1013. http://dx.doi.org/10.1111/maps.12830.

Genge, M.J., Engrand, C., Gounelle, M., Taylor, S., 2008. The classification of micrometeorites. Meteorit. Planet. Sci. 43 (3), 497–515. http://dx.doi.org/10.1111/j.1945-5100.2008.tb00668.x, arXiv:https://onlinelibrary.wiley.com/doi/pdf/10.1111/j.1945-5100.2008.tb00668.x, URL https://onlinelibrary.wiley.com/doi/abs/10.1111/j.1945-5100.2008.tb00668.x.

Genge, M.J., Grady, M.M., Hutchinson, R., 1996. Evidence in a glassy cosmic spherule from Antarctica for grazing incidence encounters with the Earth's atmosphere. Meteorit. Planet. Sci. 31 (5), 627–632. http://dx.doi.org/10.1111/j.1945-5100.1996.tb02035.x, arXiv:https://onlinelibrary.wiley.com/doi/pdf/10.1111/j.1945-5100.1996.tb02035.x, URL https://onlinelibrary.wiley.com/doi/abs/10.1111/j.1945-5100.1996.tb02035.x.

Genge, M., Larsen, J., Van Ginneken, M., Suttle, M., 2017. An urban collection of modern-day large micrometeorites: Evidence for variations in the extraterrestrial dust flux through the Quaternary. Geology 45 (2), 119–122. http://dx.doi.org/10.1130/G38352.1, arXiv:https://pubs.geoscienceworld.org/gsa/geology/article-pdf/45/2/119/3549942/119.pdf.

Glavin, D.P., Bada, J.L., 2001. Survival of amino acids in micrometeorites during atmospheric entry. Astrobiology 1 (3), 259–269. http://dx.doi.org/10.1089/15311070152757456.

Glavin, D., Matrajt, G., Bada, J., 2004. Re-examination of amino acids in antarctic micrometeorites. Adv. Space Res. 33 (1), 106–113. http://dx.doi.org/10.1016/j.asr.2003.02.011, URL https://www.sciencedirect.com/science/article/pii/S0273117703010433, Space Life Sciences: Steps Toward Origin(s) of Life.

Gough, D.O., 1981. Solar interior structure and luminosity variations. In: Domingo, V. (Ed.), Physics of Solar Variations. Springer Netherlands, Dordrecht, pp. 21–34.

Horanyi, M., Houpis, H.L.F., Mendis, D.A., 1988. Charged dust in the earth's magnetosphere. In: Fälthammar, C.-G., Arrhenius, G., De, B.R., Herlofson, N., Mendis, D.A., Kopal, Z. (Eds.), Plasma and the Universe: Dedicated to Professor Hannes Alfvén on the Occasion of His 80th Birthday, 30 May 1988. Springer Netherlands, Dordrecht, pp. 215–229. http://dx.doi.org/10.1007/978-94-009-3021-6_15.

Hörz, F., et al., 2006. Impact features on stardust: Implications for comet 81p/wild 2 dust. Science 314 (5806), 1716–1719. http://dx.doi.org/10.1126/science.1135705, arXiv:https://www.science.org/doi/pdf/10.1126/science.1135705, URL https://www.science.org/doi/abs/10.1126/science.1135705.

Hughes, D.W., Williams, I.P., 2000. The velocity distributions of periodic comets and stream meteoroids. Mon. Not. R. Astron. Soc. 315 (3), 629–634. http://dx.doi.org/10.1046/j.1365-8711.2000.03435.x, arXiv:https://onlinelibrary.wiley.com/doi/pdf/10.1046/j.1365-8711.2000.03435.x, URL https://onlinelibrary.wiley.com/doi/abs/10.1046/j.1365-8711.2000.03435.x.

Iglesias-Groth, S., Cataldo, F., Ursini, O., Manchado, A., 2011. Amino acids in comets and meteorites: stability under gamma radiation and preservation of the enantiomeric excess. Mon. Not. R. Astron. Soc. 410 (3), 1447–1453. http://dx.doi.org/10.1111/j.1365-2966.2010.17526.x, arXiv:https://academic.oup.com/mnras/article-pdf/410/3/1447/2845111/mnras0410-1447.pdf.

Jacchia, L.G., 1977. Thermospheric temperature, density, and composition: New models. SAO Special Report, 375.

Jackson, A., Zook, H., 1992. Orbital evolution of dust particles from comets and asteroids. Icarus 97 (1), 70–84. http://dx.doi.org/10.1016/0019-1035(92)90057-E, URL https://www.sciencedirect.com/science/article/pii/001910359290057E.

Johnstone, C.P., Güdel, M., Stökl, A., Lammer, H., Tu, L., Kislyakova, K.G., Lüftinger, T., Odert, P., Erkaev, N.V., Dorfi, E.A., 2015. The evolution of stellar rotation and the hydrogen atmospheres of habitable-zone terrestrial planets. Astrophys. J. Lett. 815 (1), L12. http://dx.doi.org/10.1088/2041-8205/815/1/L12.

Joswiak, D.J., Brownlee, D.E., Pepin, R.O., Schlutter, D.J., 2007. Densities and mineralogy of cometary and asteroidal interplanetary dust particles collected in the stratosphere. In: Krueger, H., Graps, A. (Eds.), Dust in Planetary Systems. In: ESA Special Publication, Vol. 643, pp. 141–144.

Kasting, J.F., 2014. Atmospheric composition of Hadean–early Archean Earth: The importance of CO. In: Earth's Early Atmosphere and Surface Environment. Geological Society of America, http://dx.doi.org/10.1130/2014.2504(04).

Kimura, H., Ishimoto, H., Mukai, T., 1997. A study on solar dust ring formation based on fractal dust models. Astron. Astrophys. 326, 263–270.

Kobayashi, K., Mita, H., Kebukawa, Y., Nakagawa, K., Kaneko, T., Obayashi, Y., Sato, T., Yokoo, T., Minematsu, S., Fukuda, H., Oguri, Y., Yoda, I., Yoshida, S., Kanda, K., Imai, E., Yano, H., Hashimoto, H., Yokobori, S.-i., Yamagishi, A., 2021. Space exposure of amino acids and their precursors during the tanpopo mission. Astrobiology 21 (12), 1479–1493. http://dx.doi.org/10.1089/ast.2021.0027, PMID: 34793260.

Koga, T., Naraoka, H., 2017. A new family of extraterrestrial amino acids in the Murchison meteorite. Sci. Rep. 7 (1), 636. http://dx.doi.org/10.1038/s41598-017-00693-9, URL https://europepmc.org/articles/PMC5428853.

Kortenkamp, S.J., Dermott, S.F., 1998. Accretion of interplanetary dust particles by the earth. Icarus 135 (2), 469–495. http://dx.doi.org/10.1006/icar.1998.5994, URL https://www.sciencedirect.com/science/article/pii/S0019103598959942.

Krivov, A., Kimura, H., Mann, I., 1998. Dynamics of dust near the sun. Icarus 134 (2), 311–327. http://dx.doi.org/10.1006/icar.1998.5949, URL https://www.sciencedirect.com/science/article/pii/S0019103598959498.

Lammer, H., Stökl, A., Erkaev, N.V., Dorfi, E.A., Odert, P., Güdel, M., Kulikov, Y.N., Kislyakova, K.G., Leitzinger, M., 2014. Origin and loss of nebula-captured hydrogen envelopes from 'sub'- to 'super-Earths' in the habitable zone of Sun-like stars. Mon. Not. R. Astron. Soc. 439 (4), 3225–3238. http://dx.doi.org/10.1093/mnras/stu085, arXiv:https://academic.oup.com/mnras/article-pdf/439/4/3225/3945778/stu085.pdf.

Larsen, J., 2016. In Search of Stardust: Micrometeorites and Other Spherules. ArtHouse DGB/Kunstbokforlaget Den Gyldne Banan.

Lasue, J., Levasseur-Regourd, A., Hadamcik, E., Alcouffe, G., 2009. Cometary dust properties retrieved from polarization observations: Application to C/1995 O1 Hale–Bopp and 1P/Halley. Icarus 199 (1), 129–144. http://dx.doi.org/10.1016/j.icarus.2008.09.008, URL https://www.sciencedirect.com/science/article/pii/S0019103508003217.

Lehmer, O.R., Catling, D.C., Buick, R., Brownlee, D.E., Newport, S., 2020. Atmospheric CO2 levels from 2.7 billion years ago inferred from micrometeorite oxidation. Sci. Adv. 6 (4), eaay4644. http://dx.doi.org/10.1126/sciadv.aay4644, arXiv:https://www.science.org/doi/pdf/10.1126/sciadv.aay4644, URL https://www.science.org/doi/abs/10.1126/sciadv.aay4644.

Love, S., Brownlee, D., 1991. Heating and thermal transformation of micrometeoroids entering the Earth's atmosphere. Icarus 89 (1), 26–43. http://dx.doi.org/10.1016/0019-1035(91)90085-8, URL https://www.sciencedirect.com/science/article/pii/0019103591900858.

Love, S.G., Brownlee, D.E., 1993. A direct measurement of the terrestrial mass accretion rate of cosmic dust. Science 262 (5133), 550–553. http://dx.doi.org/10.1126/science.262.5133.550, arXiv:https://www.science.org/doi/pdf/10.1126/science.262.5133.550, URL https://www.science.org/doi/abs/10.1126/science.262.5133.550.

Love, S.G., Joswiak, D.J., Brownlee, D.E., 1994. Densities of stratospheric micrometeorites. Icarus 111 (1), 227–236. http://dx.doi.org/10.1006/icar.1994.1142, URL https://www.sciencedirect.com/science/article/pii/S0019103584711420.

Manabe, S., Strickler, R.F., 1964. Thermal equilibrium of the atmosphere with a convective adjustment. J. Atmos. Sci. 21 (4), 361–385. http://dx.doi.org/10.1175/1520-0469(1964)021<0361:TEOTAW>2.0.CO;2, URL https://journals.ametsoc.org/view/journals/atsc/21/4/1520-0469_1964_021_0361_teotaw_2_0_co_2.xml.

Manabe, S., Wetherald, R.T., 1967. Thermal equilibrium of the atmosphere with a given distribution of relative humidity. J. Atmos. Sci. 24 (3), 241–259. http://dx.doi.org/10.1175/1520-0469(1967)024<0241:TEOTAW>2.0.CO;2, URL https://journals.ametsoc.org/view/journals/atsc/24/3/1520-0469_1967_024_0241_teotaw_2_0_co_2.xml.

Manners, J., Edwards, J.M., Hill, P.G., 2017. SOCRATES technical guide suite of community radiative transfer codes based on edwards and slingo.

Ménez, B., Pisapia, C., Andreani, M., Jamme, F., Vanbellingen, Q.P., Brunelle, A., Richard, L., Dumas, P., Réfrégiers, M., 2018. Abiotic synthesis of amino acids in the recesses of the oceanic lithosphere. Nature 564 (7734), 59–63. http://dx.doi.org/10.1038/s41586-018-0684-z.

Nesvorny, D., Jenniskens, P., Levison, H.F., Bottke, W.F., Vokrouhlicky, D., Gounelle, M., 2010. Cometary origin of the zodiacal cloud and carbonaceous micrometeorites. implications for hot debris disks. Astrophys. J. 713 (2), 816. http://dx.doi.org/10.1088/0004-637X/713/2/816.

Niimi, R., Kadono, T., Tsuchiyama, A., Okudaira, K., Hasegawa, S., Tabata, M., Watanabe, T., Yagishita, M., MacHii, N., Nakamura, A., Uesugi, K., Takeuchi, A., Nakano, T., 2012. Size and density estimation from impact track morphology in silica Aerogel: Application to dust from comet 81p/wild 2. Agron. J. 744 (1), http://dx.doi.org/10.1088/0004-637X/744/1/18.

Öpik, E.J., 1951. Collision probability with the planets and the distribution of planetary matter. Proc. R. Irish Acad. Sect. A 54, 165–199.

Öpik, E.J., 1959. Physics of meteor flight in the atmosphere. By E. J. Opik. Interscience tracts on physics and astronomy. No. 6. Ed. by R. E. Marshak. London, (Interscience Publishers), 1958. Pp. viii, 174; 14 Figs.; 55 Tables. $1.95. Q. J. R. Meteorol. Soc. 85 (365), 320. http://dx.doi.org/10.1002/qj.49708536526, arXiv:https://rmets.onlinelibrary.wiley.com/doi/pdf/10.1002/qj.49708536526, URL https://rmets.onlinelibrary.wiley.com/doi/abs/10.1002/qj.49708536526.

Rosing, 1999. 13C-Depleted carbon microparticles in >3700-Ma sea-floor sedimentary rocks from west greenland. Science 283 5402, 674–676, URL https://api.semanticscholar.org/CorpusID:22510414.

Schaefer, L., Fegley, B., 2010. Chemistry of atmospheres formed during accretion of the Earth and other terrestrial planets. Icarus 208 (1), 438–448. http://dx.doi.org/10.1016/j.icarus.2010.01.026, URL https://www.sciencedirect.com/science/article/pii/S001910351000045X.

Taylor, S., Lever, J.H., Harvey, R.P., 2000. Numbers, types, and compositions of an unbiased collection of cosmic spherules. Meteorit. Planet. Sci. 35 (4), 651–666. http://dx.doi.org/10.1111/j.1945-5100.2000.tb01450.x, arXiv:https://onlinelibrary.wiley.com/doi/pdf/10.1111/j.1945-5100.2000.tb01450.x, URL https://onlinelibrary.wiley.com/doi/abs/10.1111/j.1945-5100.2000.tb01450.x.

Uesugi, M., Uesugi, K., Oka, M., 2010. Non-destructive observation of meteorite chips using quantitative analysis of optimized X-ray micro-computed tomography. Earth Planet. Sci. Lett. 299 (3), 359–367. http://dx.doi.org/10.1016/j.epsl.2010.09.016, URL https://www.sciencedirect.com/science/article/pii/S0012821X10005911.

Volkova, T.V., Blokhina, S., Ryzhakov, A.M., Sharapova, A., Ol'khovich, M., Perlovich, G.L., 2015. Vapor pressure and sublimation thermodynamics of aminobenzoic acid, nicotinic acid, and related amido-derivatives. J. Therm. Anal. Calorim. 123, 841–849, URL https://api.semanticscholar.org/CorpusID:93277783.

Weiss, I.M., Muth, C., Drumm, R., Kirchner, H.O.K., 2018. Thermal decomposition of the amino acids glycine, cysteine, aspartic acid, asparagine, glutamic acid, glutamine, arginine and histidine. BMC Biophys. 11, 2. http://dx.doi.org/10.1186/s13628-018-0042-4, URL https://europepmc.org/articles/PMC5807855.

Yang, H., Ishiguro, M., 2018. Evolution of cometary dust particles to the orbit of the earth: Particle size, shape, and mutual collisions. Astrophys. J. 854 (2), 173. http://dx.doi.org/10.3847/1538-4357/aaab59.

Zahnle, K.J., Gacesa, M., Catling, D.C., 2019. Strange messenger: A new history of hydrogen on Earth, as told by xenon. Geochim. Cosmochim. Acta 244, 56–85. http://dx.doi.org/10.1016/j.gca.2018.09.017, URL https://www.sciencedirect.com/science/article/pii/S0016703718305349.

Zubavichus, Y., Fuchs, O., Weinhardt, L., Heske, C., Umbach, E., Denlinger, J.D., Grunze, M., 2004. Soft X-Ray-induced decomposition of amino acids: An XPS, mass spectrometry, and NEXAFS study. Radiat. Res. 161 (3), 346–358. http://dx.doi.org/10.1667/RR3114.1.